Project acronym and title:
SECURe – Subsurface Evaluation of Carbon capture and storage and Unconventional risks

D2.3 REPORT ON INDUCED SEISMICITY MODELS

Authors and affiliation:
Thomas LE GUENAN[1], Hideo AOCHI[1], Brecht WASSING[2], Thibault CANDELA[2], Jan TER HEEGE[2]

[1] BRGM

[2] TNO

Email of lead author:
t.leguenan@brgm.fr

D2.3
Revision:1

Project funded by the European Commission within the Horizon 2020 Programme	
Dissemination Level	
PU	*Public*
~~***CO***~~	~~*Confidential, only for members of the consortium (incl. the Commission Services)*~~
~~***CL***~~	~~*Classified, as referred to in Commission decision 2001/844/EC*~~

Deliverable number:	**D2.3**
Deliverable name:	**Report on induced seismicity models**
Work package:	**WP2 Risk assessment**
Lead WP/deliverable beneficiary:	BRGM

Status of deliverable		
	By	**Date**
Submitted (Author(s))	**T. LE GUENAN**	**07/05/2020**
Verified (WP leader)	J. Wollenweber	21/05/2020
Approved (EB member)	P. Cerasi	21/05/2020
Approved (Coordinator)	E. Hough	27.05.2020

Author(s)		
Name	**Organisation**	**E-mail**
T. LE GUENAN	**BRGM**	**t.leguenan@brgm.fr**
H. Aochi	BRGM	h.aochi@brgm.fr
B. Wassing	TNO	brecht.wassing@tno.nl
T. Candela	TNO	thibault.candela@tno.nl
J. Ter Heege	TNO	jan.terheege@tno.nl

Public introduction

Subsurface Evaluation of CCS and Unconventional Risks (SECURe) is gathering unbiased, impartial scientific evidence for risk mitigation and monitoring for environmental protection to underpin subsurface geoenergy development. The main outputs of SECURe comprise recommendations for best practice for unconventional hydrocarbon production and geological CO2 storage. The project is funded from June 2018–May 2021.

The project is developing monitoring and mitigation strategies for the full geoenergy project lifecycle; by assessing plausible hazards and monitoring associated environmental risks. This is achieved through a program of experimental research and advanced technology development that includes demonstration at commercial and research facilities to formulate best practice. We will meet stakeholder needs; from the design of monitoring and mitigation strategies relevant to operators and regulators, to developing communication strategies to provide a greater level of understanding of the potential impacts.

The SECURe partnership comprises major research and commercial organisations from countries that host shale gas and CCS industries at different stages of operation (from permitted to closed). We are forming a durable international partnership with non-European groups; providing international access to study sites, creating links between projects and increasing our collective capability through exchange of scientific staff.

Executive report summary

This report is part of WP2 of the H2020 project SECURe. WP2 deals with risk assessment procedures for CO_2 storage and unconventional gas operations. Amongst the various threats considered in Geoenergy projects, the risk of induced seismicity is an important one as it already leads to paused or stopped deep geothermal, shale gas or conventional gas projects and is thus one of the main concerns of stakeholders. This report deals with models for induced seismicity as a tool for assessing its risk and is designed mainly for researchers and engineers interested in risk assessment of induced seismicity.

The objectives of this report are to provide an overview of existing modelling approaches of induced seismicity, and to assess their application with real data and case studies of CO_2 storage and unconventional gas exploitation.

We present many examples of models developed for a variety of subjects: natural earthquakes, deep geothermal energy, unconventional gas exploitation, wastewater injection, and CO_2 storage. Models are grouped in three categories: statistical models, physics-based models, and hybrid models. Each type of model has its own advantages and drawbacks. Statistical models were developed for short-term forecasting and risk assessment, are fast to run and contains fewer parameters so they can be fitted with data more easily. However, they cannot provide insights into the underlying mechanisms. This is one of the main purposes of physics-based models, which are thus more adapted for longer term forecasts and risk assessment. One of the drawbacks is that the results are often deterministic and their use in risk assessment is not straightforward. They are also considerably more computationally time-consuming than the simple statistical models. Hybrid models are developed in order to find a compromise between the two approaches, where parameters of a statistical model are informed by physical parameters computed in a numerical model. This approach may be the most promising for the use in induced seismicity risk assessments as it is able to compute a risk while providing the necessary evidence for analysing the results.

A popular type of statistical model is the ETAS model. This model is tested with data from a CO_2 storage pilot and from wastewater injection in Oklahoma, USA. The analysis shows the complexity of real data and the difficulty of correlating operation parameters with observed seismicity. More work is thus needed for adapting the model to induced seismicity. It also shows that an approach not considering the full range of uncertainties will be too biased and thus detrimental in a risk assessment context.

Contents

FIGURES

TABLES

1 Introduction

Induced seismicity is one of the main concerns regarding subsurface Geoenergy projects. In particular, induced seismicity felt at the surface is a show stopper as happened for instance in Basel in the case of a deep geothermal project (Häring et al. 2008) or more recently in the UK during tests for shale gas exploitation (Energy post, 2019). Recent cases linked with unconventional gas production are, for example, detailed in Davies et al. (2013) and Porter et al. (2019).

Induced seismicity occurs when a fault or a fracture in the subsurface is subject to a change of stress which leads to its failure and a sudden release of energy. Here, we say that it is induced when the change of stress is primarily due to a change in pore pressure which is the result of subsurface exploitation such as injection of fluids (the next chapter will provide a more in depth review of the various mechanisms involved in induced seismicity). Most of induced seismicity is micro-seismicity[1]: it is part of the process of subsurface operations, and it cannot be felt at the surface. In some cases, such as deep geothermal energy, it is even necessary to correlate induced seismicity with fracture aperture, which enhances the circulation of fluids in the deep subsurface. However, when this seismicity is not monitored, analysed and managed, there is a possibility to induce larger events which can be felt at the surface. Managing this risk is thus mandatory for most subsurface geonenergy projects.

Risk assessment is the part of risk management[2] that seeks to understand the risk. In a simple form, to assess the risk is to answer these three questions (Stamatelatos et al. 2011):

1. What can go wrong?
2. How likely is it?
3. What are the associated consequences?

For the first question, we usually need to look at all the failure modes in a system and build a comprehensive set of risk scenarios. This is one of the objective of SECURe work package 2, and in particular task 2.1 “Risk assessment framework and scenario analysis”. Task 2.2 looks at the risk related to well integrity, task 2.3 to the assessment of faults and fractures potential to leak. This report is part of task 2.4 on surface deformation and induced seismicity. Specifically, we focus on the risk of felt induced seismicity provoked by subsurface operations. Regarding the third question, a preliminary answer is: nuisances at the surface, potential damage of surface infrastructure and cessation of the project. The objective of this report is to provide information and knowledge for answering the second question: how likely is it. In particular, the main topic is on modelling approaches as a tool for assessing the risk (mainly likelihood) of felt induced seismicity due to subsurface operations.

In the second chapter of this report, after a brief overview of theoretical aspects, we will provide a review of published models and modelling case studies. In the third chapter, we provide some details on some of the models. The fourth chapter deals with data analysis with the ETAS model on real case studies. The fifth chapter provides recommendations regarding the use of the models for managing risks related to induced seismicity.

[1] Micro-seismicity are events that are not felt by the population. Typically they have a local magnitude below 2. More details can be found in SECURe deliverable D2.1.

[2] SECURe project’s organisation closely follows risk management principles : work package (WP) 2 study risk assessment, WP3 and 4 deal with risk monitoring, WP5 is risk mitigation, and WP6 risk communication. All public deliverables can be accessed here: https://www.securegeoenergy.eu/

2 State of the art

This study focusses only on models to analyse induced seismicity events, i.e. the approach should be able to forecast. Purely observation-based traffic light system approaches (e.g. Bommer, 2006 or Häring, 2008) are therefore excluded, which can be used for guiding real-time decisions on field operations, but are not meant to predict future seismicity.

A wide range of approaches for modelling induced seismicity caused by varying subsurface activities has been reported in literature. These modelling approaches can give further insights in the way operational conditions and local geology, hydrogeology and mechanical characteristics of the reservoir will affect the main processes driving induced seismicity. Dominant driving processes of induced seismicity are pore pressure diffusion, poroelasticity, thermoelasticity, stress transfer and chemical changes, causing either stress changes on faults or alterations of fault properties which ultimately may cause a seismic response of the rocks. The choice and added value of a certain approach for modelling fault reactivation and/or induced seismicity will depend both on the specific question that needs to be addressed and on the timing in relation to the subsurface operations (i.e. models can be used either before, during or after the subsurface operations, e.g. for a priori assessment of seismic hazard, as component of an Adaptive Traffic Light System, or to analyze causality of observed seismicity and operations). This means that the specific choice of model type and complexity should be based on the problem at hand. As such, there is no 'best-practice' or preferred approach for modelling fault reactivation and induced seismicity related to either CO_2 injection and storage or waste water injection related to shale gas operations. Here we give a short and high-level overview of different modelling approaches for induced seismicity and shortly address the applicability and limitations of the different modelling approaches.

2.1 THEORY

Vilarrasa et al. (2019), White and Foxall (2016) or Gaucher et al. (2015) provide good overviews of the underlying mechanisms. The basic principle is that operation in the subsurface leads to pore pressure changes. This change in pore pressure leads to a variation of in-situ stress, either directly or indirectly. This variation then has the potential to shift a fault or fracture into an unstable state provoking seismicity.

In summary, the important phenomena are:

- Initial in-situ stress
- Initial state of faults and fractures (i.e. how close are they to failure)
- Pore pressure changes
- Effect on stress changes

Vilarrasa et al. (2019) highlight that stress variations are not only due to the hydraulic effect but by a variety of complex coupled factors. In particular, there are two effects which are important in understanding observations, the poroelastic effect and stress redistribution effect (Segall and Lu, 2015). The poroelastic effect describes the situation when stress is modified by redistribution of stress following pore pressure change. This effect explains why seismicity occurs also in oil and gas production where pressure decreases. The stress redistribution is due to stress drops provoked by each event, which also have the potential to trigger new events. This is the main mechanisms behind aftershocks following a larger mainshock.

These complex factors explain why modelling induced seismicity is a challenge, and why simple correlations with operational parameters do not give satisfying results for a proper risk assessment. But as in any modelling effort, a balance between increasing the complexity of the model, increasing the forecasting performance, and computational efficiency is required.

2.2 APPLICATIONS

We distinguish between two endmembers of induced seismicity models, i.e. fully stochastic and fully physics-based models. The purely stochastic (or statistical) models do not, or only to a very limited extent, incorporate the underlying physical processes and mechanisms of fault reactivation and induced seismicity. This means stochastic models, as compared to physics-based models, need only a limited number of physical parameters as input. Though generally robust and efficient, fully stochastic models rely heavily on calibration against observed induced seismicity. The stochastic approaches are often used to reproduce catalogues of observed induced seismicity in order to forecast seismic events in near real-time (Gaucher et al., 2015). This means they can be run in near real-time, for example to forecast seismic hazard in the near future in Advanced Traffic

Light Systems (ATLS). In contrast to fully stochastic models, physics-based models try to capture the main physical processes which cause fault reactivation and associated seismic events. In that sense physics-based models can increase the understanding of mechanisms causing induced seismicity and be used to explore scenarios of varying geological or operational factors. Fully physics-based models generally require more, often poorly constrained, input parameters and can be computationally intensive. In between these two endmembers, hybrid models combine physical-based and statistical approaches. To ensure computational efficiency, hybrid seismicity models aim to capture the key physical processes of induced seismicity in a simplified manner. The relatively fast hybrid models allow for a random sampling of model parameters and can be used to give probability distributions of modelling results and incorporate uncertainties in model outcome.

In this section we will review and explain the different approaches in the literature, with a special focus on risk assessment. As mentioned in the introduction, assessing the risk requires at least an element of likelihood (generally expressed as a probability), and an element of consequence. Usually models will simulate events with a given magnitude, but a magnitude is not a consequence. Ultimately, risk should be expressed as a form of loss (Bommer et al. 2015). Expressing the result in terms of ground motion or felt intensity is a good practice (Porter et al., 2019).

2.2.1 Statistical approaches

The first study that developed statistical approaches for geothermal induced seismicity was Bachmann et al. (2011), with the objective of short-term forecasting for improving the Traffic-Light System protocol. Two models are tested in this paper: The so-called Reasenberg & Jones model and the ETAS (Epidemic Type Aftershock Sequence) model. Both models were initially developed and are widely used for simulating aftershock sequences for natural earthquakes (Zhuang et al. 2012) and were adapted here by the authors for application to induced seismicity. They compare their forecasting capabilities on the data of the Basel case study in a pseudo-prospective manner. They only use flow rate as input to the ETAS model and find that this particular model performs best. An interesting aspect is that they use the models for computing probabilities of exceeding a ground motion intensity level, a step in the direction of risk assessment.

Mena et al. (2013) extended this work by adding to the two previous models a new family of models: the Shapiro model (from Shapiro et al., 2010). This model was specifically developed for injection-induced seismicity, following the observation that the number of earthquakes larger than some given magnitude increases approximately proportionally to the injected fluid volume. An interesting aspect of this paper is that the model which gives the best forecasting performance is actually an ensemble model obtained by combining the three models based on Akaike weights. Similar models have been tested also using a Bayesian framework for inferring the parameters (Broccardo et al., 2017) or in a formal decision setting in the context of Advanced Traffic Light Systems (Mignan et al. 2017).

These models propose a number of advantages for short term forecasting: as they are very fast and have relatively few parameters, it is possible to use them with data assimilation in quasi real time. This type of use would be very difficult with more complex models which can have many free parameters and are much slower to run. The obvious drawbacks are that they are not very helpful for understanding the underlying mechanisms.

In the context of wastewater injection associated with shale gas production in the Midwest US (i.e. in Oklahoma and surrounding states), Llenos and Michael (2013) have fitted an ETAS model to the data. Their conclusion is that the model does not reproduce the observation and thus the seismicity has anthropogenic origin. They however do not try a modified ETAS model taking account of injection parameters. Wang et al. (2016) use Bayesian inference to fit different non-stationary versions of the ETAS model. They find that a model with a base rate function increasing in several steps fits the observations well. The same group also extended the model to take account of spatial heterogeneity (Wang et al., 2017). The main drawback of this approach is that they do not consider injection parameters, only seismic data. This means that their particular model will not fit another dataset, even if the same type of approach is highly transposable.

Bourne and Oates (2017) also adapted the ETAS model in the context of a depleted reservoir in the Netherlands, which showed problematic seismicity due to decades of (conventional) gas production.

Langenbruch and Zoback (2016) adapted the Shapiro model to wastewater injection (associated with Shale gas production) in Oklahoma, USA. Their aim was to forecast how seismicity would change following new regulation imposing a reduction of injection rates. They introduced new parameters to account for a regional forecast.

Statistical models have also been tested in the context of hydraulic fracturing by Verdon and Budge (2018). They tested two models in a pseudo-prospective manner: the seismogenic index (or Shapiro model from

Shapiro et al., 2010) and the seismic efficiency model from Hallo et al. (2014). This last model is based on the observation that the cumulative moment release is proportional to the cumulative injected volume. However, the paper does not formally assess (e.g. with log likelihood) the forecasting capabilities of both models and it is not possible to state which model performs better. The same approach was followed by Clarke et al. (2019) on the Preston New Road case in England. They assess different versions of the seismic efficiency model by testing different scaling factors.

To our knowledge, this empirical or statistical approach has not been tested on a CO_2 storage site (White and Foxall, 2016). Chapter 4 looks at the utilisation of the ETAS model with data sets from CO_2 storage as well as shale gas exploitation.

2.2.2 Physics-based models

Many groups have developed physics-based models of induced seismicity and it is beyond the scope of this report to provide an exhaustive review. We will rather highlight more recent and/or original approaches used in the fields of CO_2 storage and unconventional gas exploitation. These applications are relatively new compared to the work of deep geothermal energy. For a comprehensive review of models used in this context: see Gaucher et al. (2015).

Induced seismicity related to unconventional gas exploitation can come from two sources: the hydraulic fracturing process itself, or wastewater co-produced with the gas that is sometimes reinjected in a deep aquifer (Mitchell and Green, 2017). As noted by Mitchell and Green (2017), physics-based modelling is very complex, requires simplifying assumptions and remains difficult and uncertain.

2.2.2.1 WASTEWATER INJECTION

Norbeck and Rubinstein (2018) developed a hydromechanical model for the case of wastewater injection in Oklahoma. They use a simple equation in order to derive the rate of stress change from injection parameters. They then use a rate-and-state friction model to relate this rate of stress change to a rate of seismicity change. They compare their forecasts with forecasts using the model from Langenbruch and Zoback (2016) and find that each model gives more accurate forecasts than the other depending on the time (e.g. onset vs post-injection).

A similar approach was followed by Dempsey and Riffault (2019): combining a simplified numerical hydrological model for predicting pressure changes, which then uses the same type of rate-and-state friction model to provide estimates of seismicity rate changes.

Recently, Zhai et al. (2019) have proposed an updated model following the same principles. They however chose a more complex geomechanical model which allows considering the poroelastic stress in addition to only pore pressure changes.

2.2.2.2 CO_2 INJECTION

In CO_2 storage, as there is very little observed seismicity, the bulk of the work in the literature consists mainly on modelling exercises in synthetic configurations, e.g. Rinaldi et al. (2014) or Mortezai & Vahedifard (2015). However, it may become a key consideration as CO_2 storage operations aim to increase injection volumes in future projects. Also, thermoelastic effects due to cooling of the storage reservoir are particularly important in case of injection of cold CO_2.

Verdon et al. (2011) built a geomechanical model of the Weyburn demonstration site. Their initial goal is not to forecast induced seismicity but rather to use the observed seismicity for constraining their model. They show that in order to better fit the observations, their geomechanical parameters were in disagreement with lab measurements, highlighting the difficulty of upscaling such measurements. The same type of workflow was also tested on the In-Salah dataset (Verdon et al., 2015) where induced seismicity data are used to check the accuracy of the geomechanical model. This model is built after history matching of observed downhole pressure.

Rutqvist et al. (2014) test a full chain model from CO_2 injection to surface ground motion. They use a hydromechanical 3D model by coupling the codes TOUGH2 and FLAC^{3}D. This approach is interesting as it allows to have a better grasp of the actual consequences. However their work is purely model-based and generic, i.e. it is not related to an actual site.

2.2.3 Hybrid models

Hybrid models were first proposed by Goertz-Allmann and Wiemer (2013) for deep geothermal energy applications. They call it hybrid because it relies on a geomechanical model that computes stress changes and uses a Mohr-Coulomb failure criterion. They use a correlation between computed stress drop and varying b values. However, they add stochastic elements to it: the initial position and stress state is randomly assigned, and a magnitude is drawn from a Gutenberg Richter (GR) relationship using the computed b-value.

This model was improved by Gischig and Wiemer (2013) mainly by adding non-linearity in the pressure diffusion aspect. A 3D extended version was checked against an improved version of the Shapiro model (see paragraph 2.2.1) by Király-Proag et al. (2016). They found that the hybrid model is generally better for the post-injection period, but the statistical model actually performed better during injection. Their approach of rigorous comparison of models is also interesting (otherwise all models give “good results” on their own).

Langenbruch et al. (2018) developed a hybrid model for the case of wastewater injection in Oklahoma and Kansas. They rely on the “Shapiro” model by computing a seismogenic index (SI). With respect to the previous work by Langenbruch and Zoback (2016) they do not consider flow rate as input but instead compute the evolution of pressure in the reservoir and the basement using hydrogeological numerical modelling. They also discretise the SI in 3D to account for heterogeneities in the distribution of faults.

2.3 ADDITIONAL THOUGHTS

This review highlights that depending on their characteristics, models have various advantages and drawbacks. In theory, the hybrid approach seems promising as it builds on the strengths of both statistical and physics-based approaches: computationally fast, stochastic assessment, underlying physical explanation. However, in practice only a rigorous benchmarking exercise on the same data set could allow to formally compare the various modelling approaches.

Here are some further thoughts on the criteria that could be used in order to judge the models:

- Speed of computation
- Complexity (number of free parameters)
- Performance in short term forecasting
- Performance in scenario forecasting (i.e. ability to model situations different than the one corresponding to the current observations)
- Representation of uncertainties

3 Presentation of the models

In this chapter we get into more details regarding the main types of models that were evoked in the previous chapter. We focus first on the statistical models before we give a more in-depth coverage of the physics-based models.

3.1 STATISTICAL MODELS

3.1.1 ETAS model

This section presents the general description of a statistical model based on Epidemic-type Aftershock Sequence model (ETAS) by Ogata (1988). The ETAS model was able to be extended as spatio-temporal model (Ogata and Zhuang, 2006). For the purpose of the injection-induced seismicity, we study a localized seismicity related to a single injection site (Case 4.1) and regional case due to many injection wells (Case 4.2). For the former, we do not consider a spatial extension. For the latter, we apply the mode by dividing many subareas. Thus, we adopt only the original ETAS model describing the temporal variation of seismicity in this study.

3.1.1.1 PRESENTATION

Figure 1 illustrates the basic concept of Epidemic-Type Aftershock Sequence (ETAS). The basic concept is that every earthquake triggers its own aftershock sequences, so that the observed seismicity is a combination of background and triggered seismicity. Ogata (1983, 1988) propose to describe this process as

$$\lambda(t) = \mu + K\sum_{t_i<t}\frac{\exp(\alpha(M_i-M_c)}{(t-t_i+c)^p} \qquad (1)$$

where the observed seismicity rate $\lambda(t)$ (generally daily earthquake numbers) is the summation of the background seismicity rate μ and the triggered part of the second term. The past earthquakes having occurred at time $t = t_i$ triggers the seismicity depending on magnitude M_i which decays with time according to Omori's law. M_c is the cut-off magnitude, above which the observed catalogue is supposed to be complete in terms of magnitude-frequency scaling (Gutenberg-Richter law) and the consequent seismicity rate is calculated for earthquakes of magnitude $M \geq M_c$. There are five parameters $(\mu, \mathrm{K}, \alpha, c, p)$ to be determined from the given seismicity catalogue. In other words, we can calculate the forecast of the seismicity once these parameters are given.

The principal difficulty for induced seismicity is that the parameter μ may not be stationary and characterizing its temporal change is a research topic in itself. There would in principle be two possibilities:

1) **Assume the stationarity of the seismicity in a limited period.** This approximation can be possible if there are sufficient earthquakes.
2) **Describe the form of μ by any equation**, $\mu = f(t; P, V)$, which can be an equation of time but also a function of operational factors such as pressure P and volume V.
   a) **Post-injection phase** for which P, V does not evolve any more (Maury et al. 2019). For such case, the background seismicity is expected to decrease gradually.

$$\lambda(t) = \mu_0 + \mathrm{B}\cdot\exp(-\gamma(t-t_S)) + K\sum_{t_i<t}\frac{\exp(\alpha(M_i-M_c)}{(t-t_i+c)^p} \qquad (2)$$

   where $(\mu_0, \mathrm{B}, \gamma)$ are free parameters and t_S is the time of end of injection (known). At the end of the injection the background seismicity has a rate of $(\mu_0 + \mathrm{B})$ and then this decreases to μ_0.

   b) **During the injection** when (P, V) may influence directly the seismicity. For example, one can assume that Coulomb stress change may trigger the background seismicity such as

$$\lambda(t) = \mu_0 + D\times\Delta CFF + K\sum_{t_i<t}\frac{\exp(\alpha(M_i-M_c)}{(t-t_i+c)^p} \qquad (3)$$

   where the Coulomb stress change is calculated by shear and normal stresses as $\Delta CFF = \tau_{shear} + \mu_f\tau_{normal}$ (μ_f is the frictional coefficient).

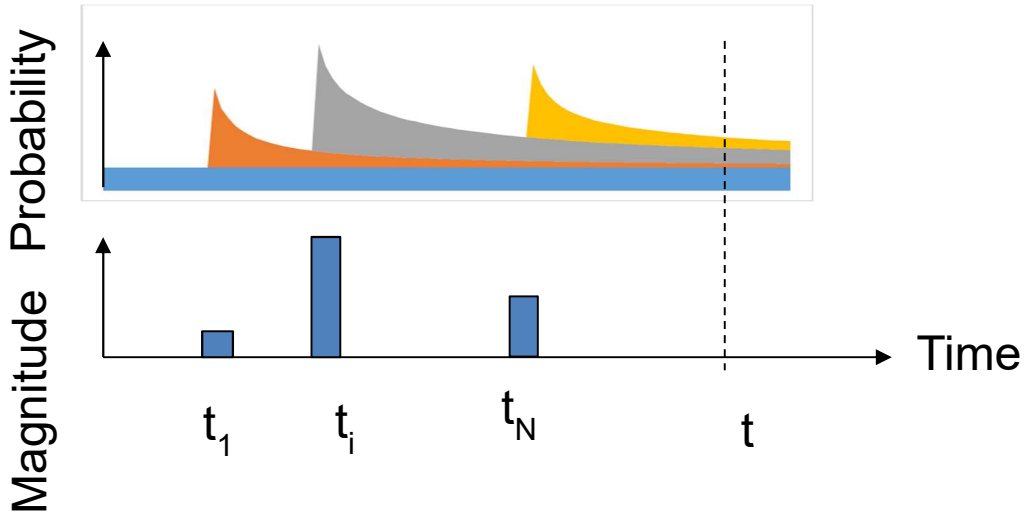

Figure 1: Basic concept of Epidemic-Type Aftershock Sequence (ETAS) model. Every earthquake triggers its own aftershock sequences governed by Omori law.

3.1.1.2 MODELLING

The ETAS model (as most statistical models of earthquakes) is based on a Poisson process with a time varying rate $\lambda(t)$ (Zhuang et al. 2012). The main principle for modelling such a process is to consider the integral of the conditional intensity:

$$\Lambda(t) = \int_0^t \lambda(t)dt$$

We then consider the time change $\tau = \Lambda(t)$ from t to τ, then $\{t_i\}$ is transformed one-to-one into $\{\tau_i\}$. Then, $\{\tau_i\}$ has the distribution of a stationary Poisson process of intensity 1 (Ogata, 1988).

Remembering that the distribution of inter-times in a Poisson process follows an exponential distribution, this useful result allows us to use the following algorithm for performing forward modelling of ETAS (or any model with time varying intensity rate):

1. Define the parameters θ; in the case of the ETAS model it is $\{\mu; K; \alpha; M_C; c; p\}$
2. $\tau_0 = 0; \Lambda(t) = \mu$
3. Sample r from an exponential distribution of rate 1
4. $\tau_i = \tau_{i-1} + r$
5. Solve for t_i the following equation: $\Lambda(t_i) = \tau_i$
6. Draw the corresponding magnitude from Gutenberg-Richter's law with a predefined β: $\Pr(Mag > M) = e^{-\beta M}$
7. Compute $\Lambda(t)$ for $t > t_i$
8. Repeat from step 3 until an ending condition is met.

3 remarks:

- $\Lambda(t)$ is straightforward to compute but the form will be different whether $p = 1$ or not.
- Step 4 is complex (impossible?) to do analytically so a root-finding numerical method is used instead
- Magnitudes are considered independent from rates. Actually, the risk increases with the rates only because by having more events it becomes more probable that a bigger one would "come out".

This algorithm was coded using standard scientific Python libraries. An example of a simulation with typical parameters (taken from Ogata, 1988) is displayed below.

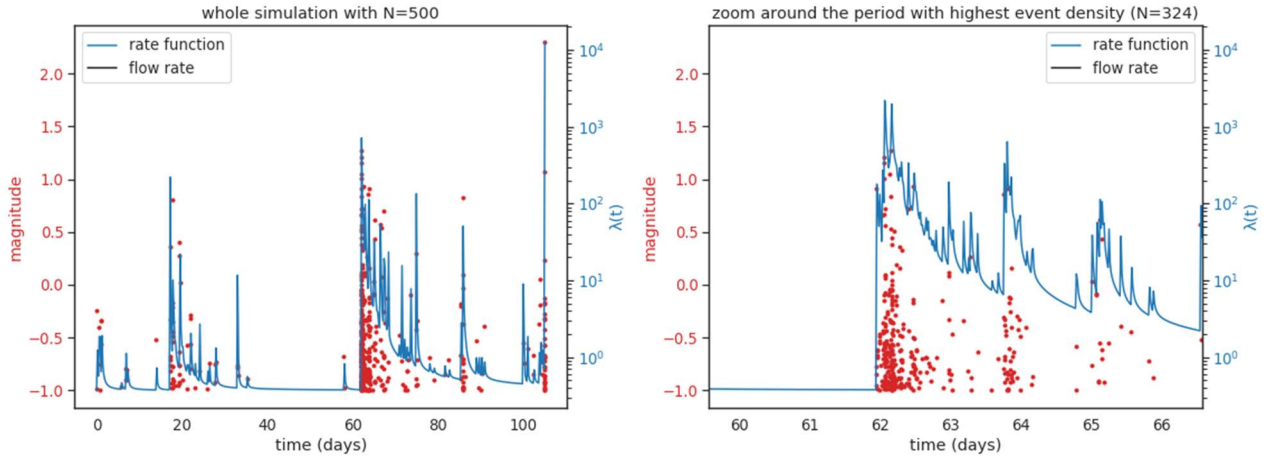

Figure 2: Simulation of the ETAS model. Red dots are the simulated events; the blue line is the corresponding intensity rate $\lambda(t)$. Left figure is the whole simulation; on the right is a zoom on the period with the highest density of events. Flow rate is 0 and is not visible on the figure

We can see in this figure the effect of largest events on the rate function. Note here that no injection parameters have been introduced so this corresponds to a simulation of natural earthquakes.

We can simulate induced seismicity by changing the base rate μ in the following way (Bachmann, et al. 2011):

$$\mu = \mu_0 + c_f F_r(t)$$

Where μ_0 is a constant rate, $F_r(t)$ is the injected flow rate, and c_f is a free parameter. The previous algorithm can then be used in a similar way by providing c_f and $F_r(t)$ or actually: $\int_0^t F_r(t)$. An example is shown below.

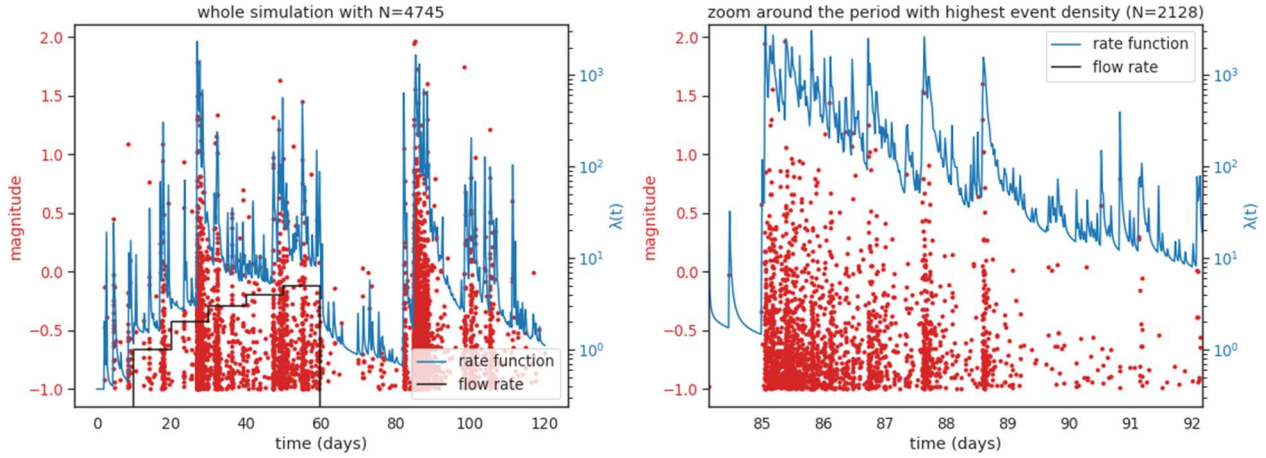

Figure 3: Example of the ETAS model for induced seismicity. Red dots are simulated events, blue line is the intensity rate, and black line is the flow rate. Injection starts at day=5 and stops at day=60; left figure is the whole simulation (t=120 days), and right figure is a zoom on the period with the highest density of events

Note that the simulated magnitudes are relatively low. It is also interesting to see that, while the intensity rate increases with injection in the first period ($t < 60$), the biggest spike happens in the post-injection period ($t > 60$). This is a good example of the inherent randomness of this model, where a "big" event might occur at any moment. This is a good illustration of the difficulty of predicting induced seismicity because there are multiple phenomena involved at the same time and some are very uncertain (in this simulation, it would be the redistribution of stresses following moderate earthquakes).

3.1.1.3 PARAMETER ESTIMATION

The five independent ETAS model parameters (Equation (1)) are often calculated with Maximum Log-Likelihood approach with a given catalogue (Ogata, 1988). For a Poisson process, the Log Likelihood is given by:

$$\log L(\theta) = \sum_{i=1}^{N} \log \lambda(t_i;\theta) - \int_0^T \lambda(t;\theta)dt$$

Where $\lambda(t;\theta)$ is the conditional intensity rate, and $\{t_i\}$ is the set of occurrence times of earthquakes in an observed time interval $[0,\ T]$.

This is a nonlinear, iterative regression based on initial guesses. Thus, we need to run many calculations in order to assure the convergence. It is worth noting that

- μ is simply (number of earthquakes)/(period of observation) without triggering term.
- K cannot be so small comparing to μ. If the triggering effect is ignored within the regression, it is possible that the solution is not obtained correctly.
- α is expected to be slightly larger than 1 such that large earthquakes play a more significant role triggering the following earthquakes. If a small α is obtained ($\alpha \sim 0.1$), the dependency of magnitude is not detected, partially because magnitude in the catalogue may be imprecise.
- c can be small, noting $c = 0$ in the original form of Omori's aftershock law. Regarding the probabilistic aspect of the process, this term might not play a principal role in the Equations.
- p is close to 1, as shown in many papers.

3.1.2 Seismogenic index model

3.1.2.1 DESCRIPTION

The seismogenic index model – sometimes called the Shapiro model – was first proposed by Shapiro et al. (2010). The main principle behind this model is the observation that there is an approximately linear dependence between the number of events above a given threshold and the cumulative injected volume.

Based on this, they define a seismogenic index Σ as a quantity independent of injection time and of any other injection characteristics. Once it has been measured for an injection site, it can be used with the following equation:

$$\log N = \log Q_c(t) - bM + \Sigma$$

With N the number of events with magnitude superior to M, $Q_c(t)$ the cumulative injected volume and b, the *b*-value in the Gutenberg-Richter (GR) distribution.

As with all the statistical models, this equation is used in a (nonhomogeneous) Poisson process for generating events. A standard power distribution based on the GR law will assign the respective magnitudes.

However this equation is only valid during injection. For the post-injection period, it is common to use a modified version of Omori's law (e.g. Langenbruch & Zoback, 2016):

$$R(t) = \frac{R_0}{\left(\frac{t}{t_0}\right)^p}, \qquad t > t_0$$

With t_0 the time at which injection stops, R_0 is the seismicity rate at injection stop, $R(t)$ is the seismicity rate at time t, where p is the p-value of Omori's law describing the rate of decay.

One of the main differences between this model and the previous ETAS model is that this one does not take account of aftershock effects: the fact that a non-negligible part of the seismicity rate is due to aftershock activity after a (bigger) main shock. In order to overcome this, most authors will calibrate the model on declustered data (i.e. aftershocks being removed from data, van Stiphout et al. 2012). This can be problematic in a real-time setting, depending on the importance of aftershocks in the sequence.

3.1.2.2 EXAMPLE

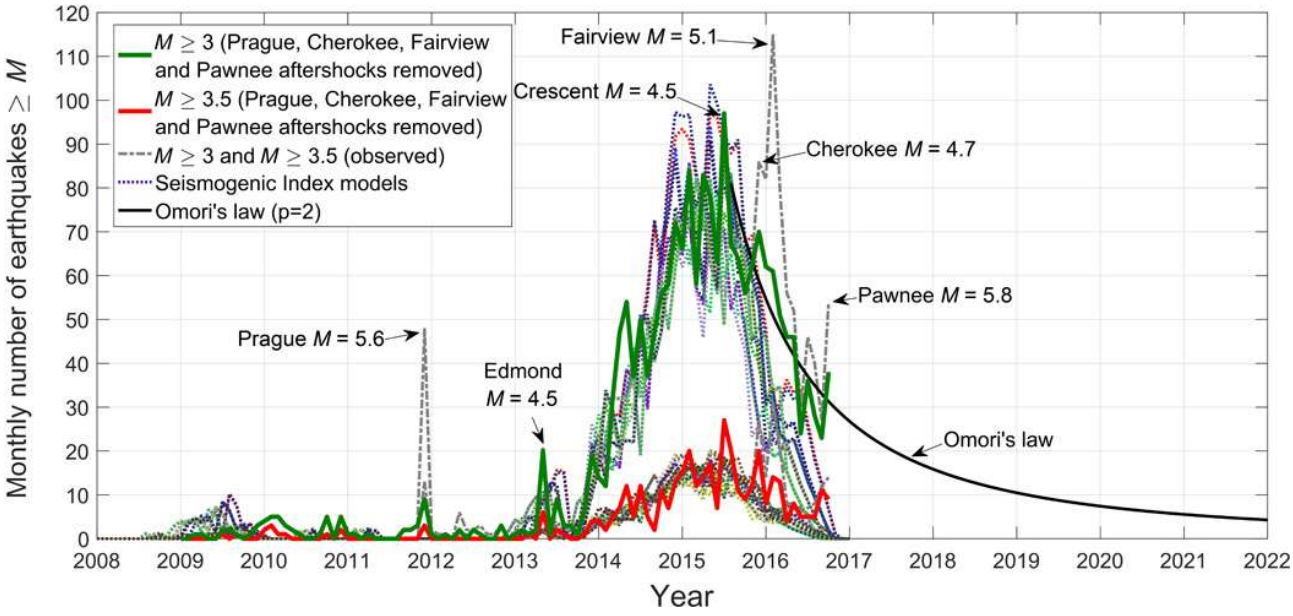

Figure 4: example of forecast using the seismogenic index (from Langenbruch & Zoback 2016)

Compared to simulations using ETAS, a forecast using the seismogenic index will appear "smoother". We can see from the example above that the large rate of seismicity following the Fairview event is not replicated by the model.

3.1.3 Seismic Efficiency Model

A similar model, called the seismic efficiency model was proposed by Hallo et al. (2014). McGarr (2014) proposed that the cumulative seismic moment released during injection ΣM_0 is determined by the total cumulative volume of fluid injected:

$$\Sigma M_0 = 2\mu V_T$$

In which μ is the rock shear modulus. This corresponds to a worst-case scenario where all the strain induced by a volume change is released as seismic energy. Hallo et al. (2014) therefore define a seismic efficiency ratio S_{EFF}. The above equation thus becomes:

$$\Sigma M_0 = S_{EFF}\mu V_T$$

From there, using the G-R relationship, the authors can link this cumulated seismic moment to the maximum magnitude induced. As with the previous model, it does not consider aftershocks or triggered events.

This model is used by Verdon & Budge (2018) in comparison with the seismogenic index model on the case of hydraulic fracturing. In fact, one model (the seismogenic index) scales the injection volume to the number of events larger than a given magnitude, while the other (the seismic efficiency) scales the injection volume to the cumulative seismic moment release.

3.2 PHYSICS-BASED MODELS

In this section we will give a high-level overview of the some of the main features and components of physics-based (and hybrid) modelling approaches, which can be applicable to modelling induced seismicity in case of CO_2 injection or wastewater-injection related to shale gas operations.

A (partially) physics-based approach to model induced seismicity associated to subsurface operations generally consists of the following (combination of) components:

1) Assessment of the spatial and temporal evolution of pressure and temperature (and in some cases also chemical processes)
2) Assessment of the spatial and temporal evolution of stress, in terms of magnitude and areal extent of fault Coulomb stress changes, fault Coulomb stressing rates and fault reactivation potential

3) Assessment of seismic or aseismic fault slip and fault rupture for a single event and/or:
4) Assessment of seismicity rates and frequency magnitude relations for multiple seismic events

Physics-based models can comprise models ranging from simplified 1D to full 3D full field models, capturing the geological complexity of the site, from analytical to numerical models and from one-way coupled to fully coupled thermo-hydro-mechanical-chemical models, capturing the complex interaction between flow, thermal, chemical and mechanical processes.

3.2.1 Modelling pressure and temperature fields

Pore pressure and temperature changes caused by injection of CO_2 or waste water injection may lead to fault reactivation and induced seismicity. In order to assess the potential of fault reactivation and enable mitigation, it is crucial to understand the interplay between faults and pressure-, temperature- and associated stress changes near these faults. The evolution of pore pressure and temperature fields can be modelled analytically, semi-analytically or numerically. Analytical solutions can be applied for simplified geometries, such as axi-symmetrical or horizontally layered (pancake-like) reservoir configurations. In the SECURe project, such an axi-symmetrical analytical model is used to model the pore pressure, temperature and stress evolution around a single injector (e.g. CO_2 injector or waste water injection well), in order to assess the impact on fault stability and seal integrity (see Figure 5). A more detailed description of the model basics and results will be presented in the deliverables D2.5 and D2.6 of the SECURe project. In Fokker et al., 2019 another example of a semi-analytical fully coupled fast model is presented which can be used to obtain a first order assessment of pore pressure, temperature and stress changes around a single injection well.

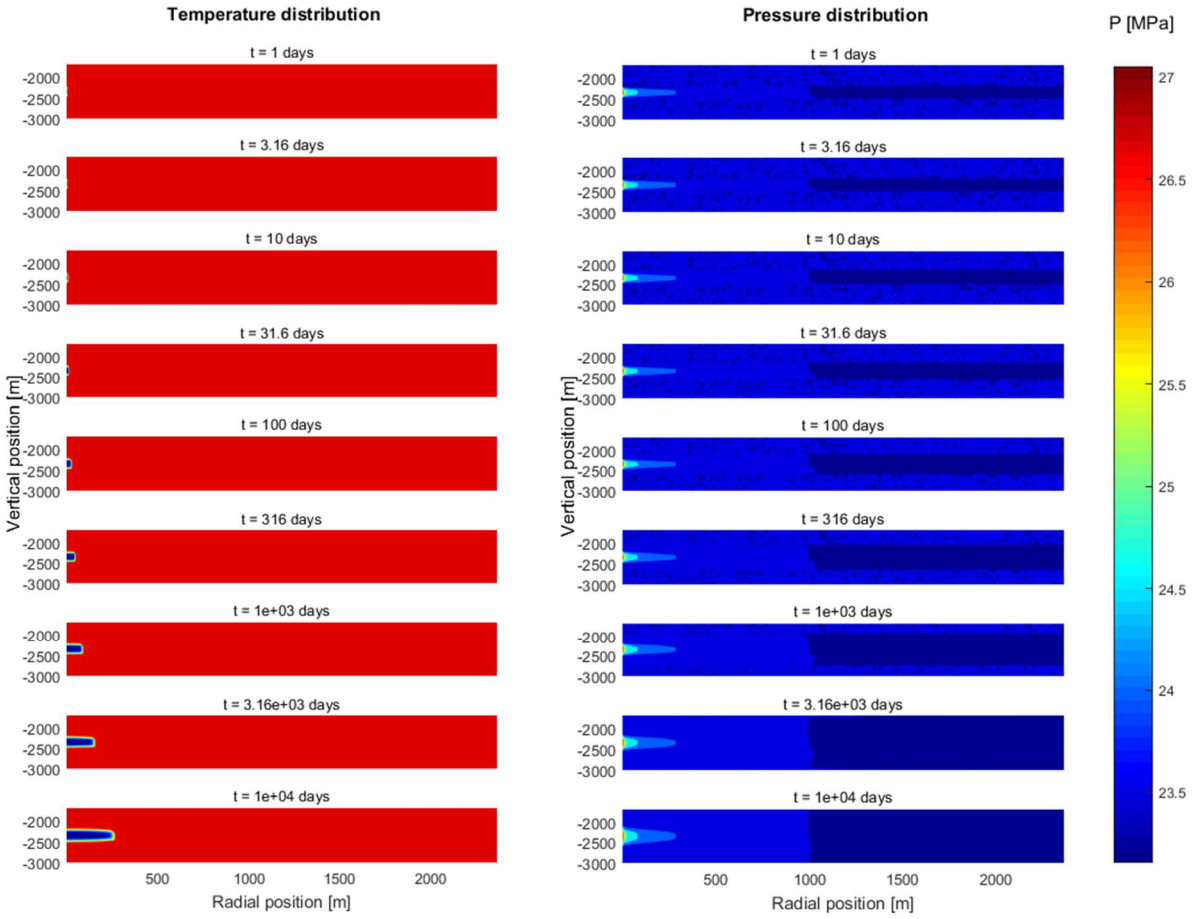

Figure 5: Axi-symmetrical analytical model of pressure and temperature evolution around an injection well.

These (semi-)analytical models will typically be used when only limited information is available on the location, orientation, offset and (sealing) properties of the faults and the geometry and properties of the reservoir and burden. (Semi-) analytical models are fast and therefore well suited for uncertainty analysis and probabilistic assessments, but they cannot fully capture the key processes and geological complexity, often relevant for large scale CO_2 or waste water injection. Pore pressure and temperature fields around multiple injection wells will deviate from radial symmetry, and heterogeneities and flow anisotropy caused by different lithologies, layering, fault offset and sealing faults cannot easily be incorporated in these simplified models. These effects can be captured in semi-analytical and numerical reservoir models. In section 3.2.5, we will shortly describe the coupled numerical model (Tough-FLAC^{3D}) which is currently used in SECURe for the assessment of fault reactivation and induced seismicity during CO_2 injection.

3.2.2 Modelling stress and fault reactivation potential

Fault reactivation potential can be evaluated using static geomechanical models, which analyze the stress evolution in the reservoir and associated effects at fault planes, based on pore pressure and temperature changes obtained from reservoir models (e.g., Ter Heege et al., 2018). As a first order screening tool, 1D analytical models for fault stability can be used to assess fault reactivation potential. These models are based on 1D uniaxial analytical solutions for poro- and thermoelastic stress changes (see e.g. Buijze et al., 2019a) caused by pressure and temperature changes. Based on fault orientation, the effective normal and shear stress changes on the faults are derived. Fault stability criteria such as slip tendency or Shear Capacity Utilization (SCU), based upon a Mohr Coulomb failure criterion, are then used to assess whether stress changes exceed fault strength, thereby causing fault reactivation. These 1D models require a minimum of input data and are very efficient in terms of computational costs, and can provide a first-order estimate of fault stability under changing pore pressure and temperature conditions. As the models are computationally efficient, they can be used for uncertainty and sensitivity analysis. They require input on initial stress conditions, elastic reservoir properties, fault orientation and fault strength to calculate fault stability and reactivation potential. Walsch and Zoback (2016) have used such a 1D fault stability model to perform a probabilistic analysis of potential fault slip related to waste water injection in Oklahoma. They incorporate uncertainties in the stress tensor, pore pressure, fault friction coefficient and fault orientation to obtain a cumulative distribution function of the pore pressure changes required to cause fault slip on each fault mapped in the area. This way, they can assess the probability of fault reactivation for each known fault in the area affected by the pressure changes induced by waste water injection.

As 1D analytical fault stability models are based on the assumption that stress changes occur under uniaxial deformation, they cannot account for the effects of spatially varying pressures and temperature fields, reservoir heterogeneity, and the effects of 'stress arching' caused by fault offset, reservoirs of limited extent and sealing faults. In contrast to 1D fault stability models, 2D and 3D semi-analytical and numerical fault stability models can be used to simulate the effect of spatial gradients in pore pressure and temperature (Ter Heege et al., 2018), and geometrical complexity on stress arching (albeit in case of 2D models the analysis is limited to ''plane strain' conditions). In Candela et al. (2019a), 3D numerical flow calculations have been combined with the 3D semi-analytical code of MACRIS (Mechanical Analysis of Complex Reservoir Induced Seismicity) to assess fault stability and associated seismicity during depletion of the Groningen gas field. In SECURe, the same MACRIS model has been used to model fault Coulomb stress changes and associated seismicity on basement faults related to waste water injection in Oklahoma (for more details see section 3.2.6).

3.2.3 Modelling fault rupture and seismicity

Fault stability models focus on the fault stress changes and their effect on fault reactivation potential. Accordingly, these models can provide valuable information on the timing and location of fault reactivation. The criteria for fault stability (such as slip tendency and SCU) in the above models are based upon a Mohr Coulomb failure criterion, which defines the 'static' strength of a fault. The Mohr-Coulomb criterion represents an ideal plastic failure criterion which cannot be used for realistic simulation of the post-failure behavior of faults. As such it cannot be used to determine the magnitude of fault slip and areal extent of fault reactivation, nor to address the question whether we can expect seismic or aseismic slip to occur. Furthermore, the above quasi-static numerical models cannot account for the effects of inertia forces, related to the (de)acceleration of the rock mass during fault rupture.

Dynamic rupture models do include the effects of inertia on fault slip and are used to investigate the time-dependent evolution of the seismic fault rupture process (Buijze et al., 2015 Wassing et al., 2016, Jin and Zoback, 2018, Buijze et al., 2019b). They are commonly based on advanced constitutive laws for fault frictional behavior, like a slip-weakening or rate and state friction law (Dieterich, 1994). These material laws are better suited for modelling the post-failure behavior of faults after the onset of fault slip. Dynamic rupture models are thus tailored to give insight into the dynamic rupture behavior of the fault. Dynamic rupture models can be used to analyze what factors control (seismic or aseismic) rupture velocities and rupture arrest, the size of the rupture area, the total slip displacements and typical stress drops of seismic events. This way they can be used to analyze if fault rupture can potentially extend outside the area of pressure and temperature disturbance and whether there is a potential for large-magnitude seismic events. Dynamic rupture models are computationally expensive and in practice mainly run in 2D to simulate the characteristics of a single seismic event. As such, they cannot provide frequency-magnitude relations of seismic events, nor can they be used to create synthetic catalogues of seismic events. An additional limitation of the models is that the input parameters for the advanced fault friction laws are usually poorly constrained. However, based on scenario and sensitivity analysis, taking into account uncertainties in input parameters, they can provide valuable insight into the main factors controlling the physics of nucleation, propagation and arrest of seismic events. It is noted here that dynamic rupture models have not been used in SECURe to model seismicity related to CO_2 or waste water injection.

3.2.4 Modelling seismicity rates and frequency magnitude relations (multiple events)

In contrast to numerical fully dynamic rupture models, hybrid approaches have been used to model frequencies and magnitudes of multiple seismic events, combining key physical processes in a simplified manner with statistics. A common approach is to use 'fast' geomechanical models to compute Coulomb stress changes on faults, combined with statistical and stochastic sampling approaches from predefined frequency-magnitude distributions to derive synthetic seismic catalogues. As an example, Gischig and Wiemer (2013) describe a hybrid model for induced seismicity around an injection well, based on a simplified 2D axisymmetrical pore pressure diffusion model, combined with a stochastic geomechanical seed model. In this seed model potential earthquake locations are represented as 'seed-faults' which are uniformly and randomly distributed over the entire model. Local in-situ stress conditions and fault orientations are drawn from a probabilistic distribution. The combination of local in-situ stress, fracture orientation and fault strength (defined by a Mohr Coulomb failure criterion) determine the fault criticality at each seed fault. Depending on the pressure-induced stress-change a fault at a certain seed-fault can reactivate and trigger a seismic event. Once an event is triggered, a magnitude is randomly drawn from a set of magnitudes forming a frequency magnitude distribution. This geomechanical seed model enables fast computation of catalogues of seismic events. Other approaches have been used to model frequency-magnitude distributions, synthetic catalogues of seismic events and/or total seismic moment released during subsurface operations. Van Wees et al. (2019) used the semi-analytical MACRIS model to assess the total seismic moment of induced seismicity caused by pore pressure changes during geothermal operations (see also section 3.2.6 for the application of MACRIS in SECURe). From on-fault positive Coulomb stress changes, they derive average excess Coulomb stress relative to a Mohr Coulomb failure law over a certain slip length. Crack theory by Madiaraga (1979) is then applied to relate seismic moment to crack size and stress drop and to compute the total seismic moment released on the fault. Several other approaches for modelling multiple seismic events have been described e.g. by Baisch et al., 2010 and Candela et al., 2019b.

In the approaches above, elastic Coulomb Stress ***Changes*** are used to derive seismicity and seismic moment release. Alternatively, a relation between Coulomb Stressing ***Rates*** and seismicity rates (rate-and-state seismicity Dieterich (1994)) can be used for modelling seismicity. Segall and Lu. (2015) and Heimison and Segall (2018) use a simplified version of rate-and-state seismicity, to relate the relative seismicity rate (defined as the ratio of the rate of seismicity to the tectonic background seismicity rate) to the Coulomb Stressing Rate. In a similar way, this relation between Coulomb Stressing Rates and seismicity rates was used by Zhai et al.(2019) and Candela et al. (2019) to model induced seismicity by waste water injection in Oklahoma, respectively seismicity induced by gas depletion in the Groningen Field. In the present SECURe project, we use a coupled numerical code in FLAC3D-Tough3 in combination with the rate-and-state seismicity theory to assess the effect of CO_2 injection in a depleted gas reservoir on induced seismicity (see next section). A more

detailed description of the model basics and results will be presented in the deliverables D2.5 and D2.6 of the SECURe project.

3.2.5 Modelling induced seismicity with a coupled Thermo-Hydro-Mechanical model in FLAC^{3D}-Tough(React)

In SECURe, we use a coupled thermo-hydro-mechanical numerical model to analyze the effect of fluid (e.g. CO_2 or water) injected into a depleted reservoir. Using the FLAC^{3D}-Tough(React) simulator (Taron et al., 2009), we take into account the coupling between the thermal, hydraulic and mechanical processes which affect pressure and temperature evolution around a single injection well and the mechanical response of nearby fault systems (see Figure 6). The FLAC3D-Tough(React) simulator is used to analyse the spatial and temporal evolution of pore pressures, temperatures and stresses in reservoir and over- and underburden around the injection well. Fault planes are not explicitly modelled, but we assume faults can be potentially present at any location in the model. Assuming a specific fault orientation and strength, the spatio-temporal evolution of pore pressures and stress changes at all locations in the model can be monitored and used to compute normal- and shear stresses on potential faults. From changes in fault normal and shear stress, Coulomb stress changes on the faults can be derived:

$$\Delta\tau_{cs} = \Delta(\tau_s - \mu\sigma'_n) \qquad [1]$$

Where the symbol Δ denotes a change, τ_s is shear stress, σ'_n is normal effective stress on the fault, σ_n is total normal stress on the fault and μ is friction coefficient of the fault. A positive Coulomb stress change indicates a destabilizing stress path of the fault, whereas a fault segment with a negative Coulomb stress change is stabilizing.

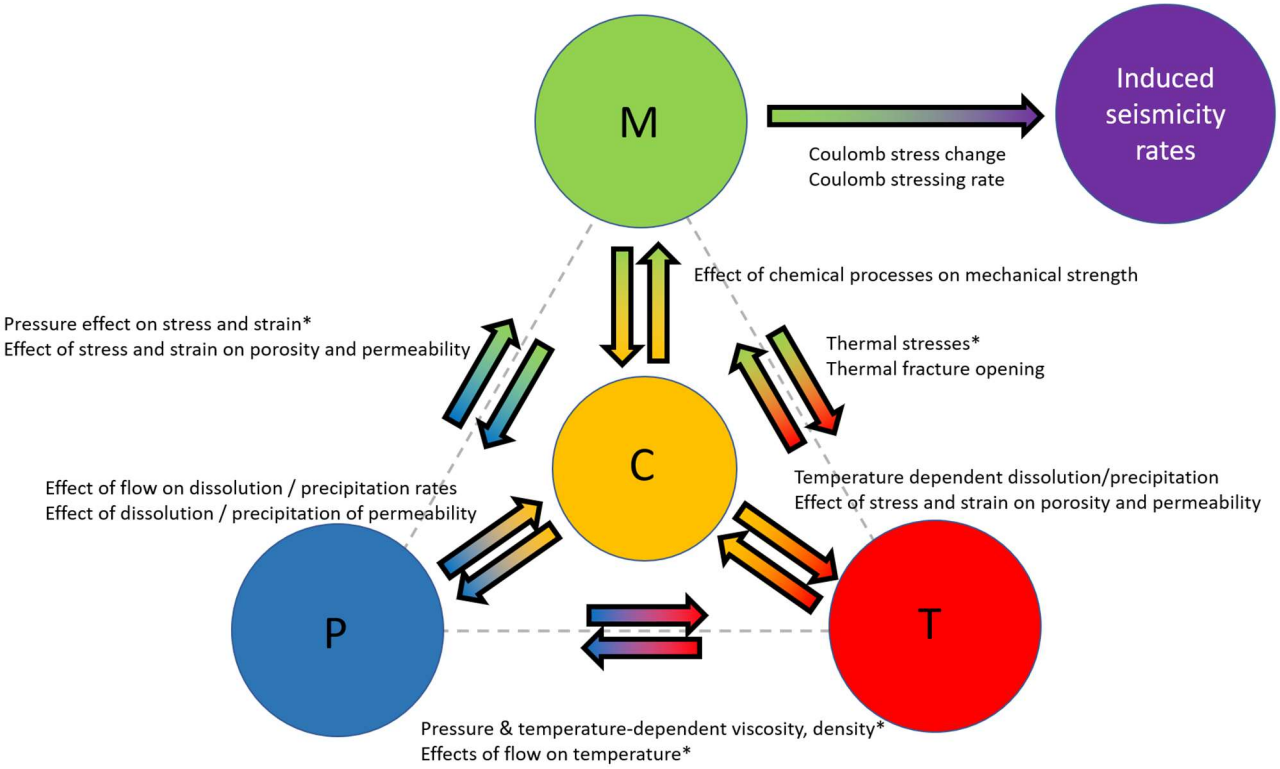

Figure 6: Schematic presentation of the interaction and coupling between processes that can play a role during fluid (e.g. CO_2, water) injection. All processes can be captured in the FLAC^{3D}-Tough(React) model. M: mechanics, T: thermal, H: hydraulic, C: chemical processes. Processes that are expected to be dominant for injection into a depleted sandstone reservoirs have been marked with an asterix. Though chemical processes can be part of the analysis, in the present SECURe project the interaction of chemical processes with flow and mechanics has not been taken into account, which means the ToughReact part of the model has not been used.

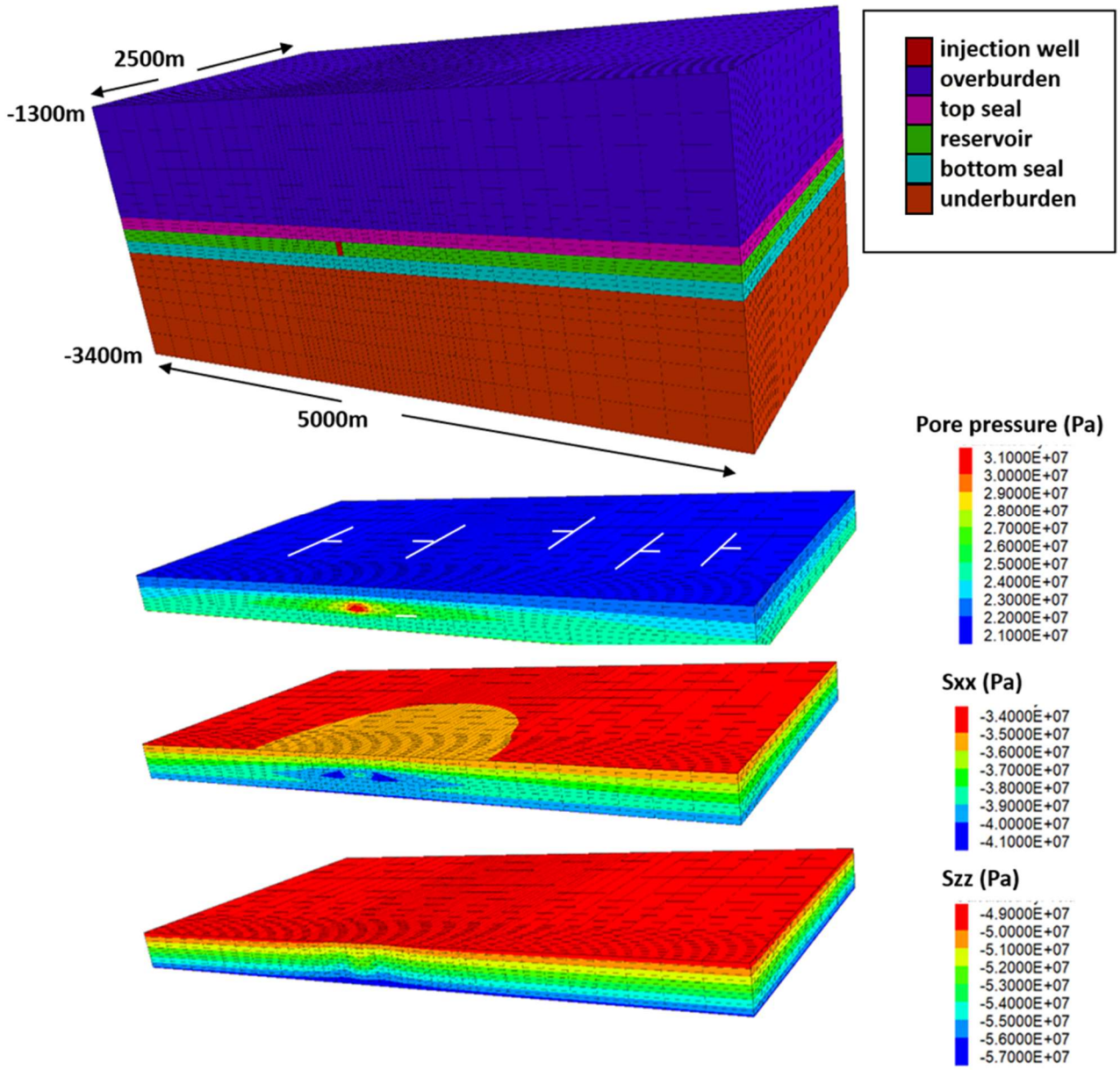

Figure 7: Example of FLAC3D-Tough(React) modelling results (half-symmetry) of fluid injection. Top: Model geometry and lithologies and position of injection well. Below, pore pressure field, total horizontal stress and total vertical stress due to pore pressure and temperature changes (not shown) after 30 years of injection. White symbols indicate potential location of faults.

The evolution of Coulomb stress changes over time can be used to derive Coulomb stressing rates. These stressing rates are then used to obtain relative seismicity rates, based on the theory of rate-and-state seismicity (Dieterich 1994, Segall et al., 2015, Heimison et al., 2018):

$$\frac{dR}{dt} = \frac{R}{t_a}\left(\frac{\dot{\tau_{cs}}}{\dot{\tau_0}} - R\right) \qquad [2]$$

Where R is relative seismicity rate (i.e. the seismicity rate divided by background seismicity rate) and $\dot{\tau}_0$ is the background tectonic stressing rate. The t_a in the above equation is a decay parameter, which defines how long it takes for seismicity to decay to its background value, following a large stress perturbation and depends on

background stressing rate, fault parameter A which quantifies the direct effect of rate and state friction behaviour of the fault and normal effective stress:

$$t_a = \frac{A\dot{\tau}_0}{\sigma_n'} \qquad [3]$$

The FLAC^{3D}-Tough(React) model in SECURe is currently applied for analysis of the effect of fluid injection into a depleted reservoir. By using this model, we analyze the impact of current and past operational parameters (such as current injection rates, volumes injected and injection temperature, past reservoir depletion pressure and its effect on stress paths during repressurization of the reservoir) and geological factors (such as reservoir and fault geometry, reservoir and seal geological, thermal, flow and mechanical properties) on fault reactivation potential and associated seismicity. Results of the FLAC3D-Tough(React) model will be described in SECURe deliverables D2.5 and D2.6..

3.2.6 Workflow for managing seismicity risks developed by TNO

TNO's objective for related work in SECURe WP5 on mitigation methods is to build a dual-objective optimization workflow (see Figure 8) for maximizing the reservoir performance while minimizing seismic activity (see initial study, described in Ter Heege et al., 2018). TNO decided to focus on the Oklahoma waste water injection case because it gathers all the required ingredients to test our workflow over a real case:

(i) a sufficient number of induced seismic events to calibrate our forward models,
(ii) a mitigation procedure imposed by the regulator,
(iii) a time period post- mitigation procedure long enough to show a statically significant seismicity response and to test the predictions of our optimization workflow.

This combination is unique, and the idea is to test the method in a pseudo-prospective way on this dataset so we can gain confidence for using it on prospective sites in Europe.

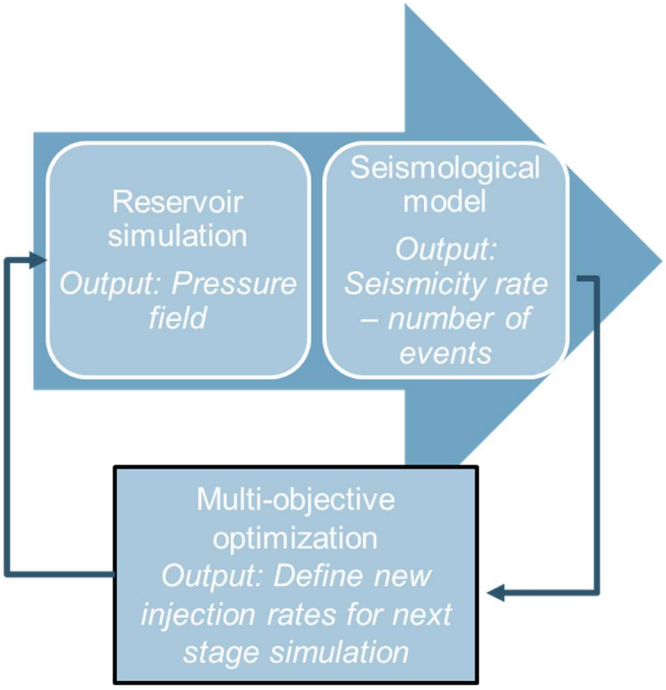

Figure 8: flowchart of the dual-optimizer

The ultimate goal is to focus on the post-mitigation procedure period and to provide relevant information to those involved with understanding risks associated with maximizing total injected volume while minimizing seismicity (over a fixed period of time). One foresees that this optimal strategy would have permitted a higher total injected volume (over a fixed period of time) with a lower seismicity risk relatively to the actual scenario (following the mitigation procedure imposed by the regulator). Detailed results of the dual-objective optimization workflow to waste water injection in Oklahoma will be reported in D5.6.

4 Case studies

In this chapter we focus on the ETAS model (section 3.1.1) and we test its application to 2 case studies: the first is from a CO_2 storage pilot site is France. The injection was in one (closed) reservoir through one well and is thus a good example of local induced seismicity. The second case study is wastewater injection in Oklahoma (USA) in relation with shale gas exploitation. Injection is in a large reservoir through hundreds of wells is thus a good example of regional induced seismicity. From the review of Chapter 2, it seems that statistical models were never applied to CO_2 storage, and there are very few application of the ETAS model to the context of unconventional gas exploitation.

4.1 CASE STUDY 1 – ROUSSE, FRANCE

4.1.1 The data

The Rousse CO_2 injection experiment was carried out in a depleted gas reservoir in the Pyrenean-Lacq area during 2010 – 2013. The reservoir context and injection process are summarized by Thibeau et al. (2013). The microseismicity observation was made around the well and well documented in Payre et al. (2014). The seismicity data is derived from Payre et al. (2014). The observed microseismicity is grouped in two categories: around the well (reservoir) and neighbouring natural earthquakes in a known fault zone. We focus only on the first induced events. As the seismicity remains relatively small and concentrated around the well, we do not use the spatial information of the seismicity; we are interested only in the magnitude-time diagram (Figure 9).

The injected volume is moderate (50 kt of CO_2 in total) and the induced seismicity is relatively low (only two events above magnitude 0, and an average rate of 0.27 observed events per day). Microseismicity of small magnitude is detected thanks to the dense, borehole network (Payre et al., 2014). During about 3 years, more than 600 micro earthquakes were detected. According to the magnitude-frequency diagram (Figure 9), we know that the completeness is down to magnitude -1.5 and 336 events (magnitude ≥ -1.5) are available for our analyses. Payre et al. (2014) propose that there are two phases of injection process. (1) main injection period: March 2011- February 2013) and (2) post-injection period (later than March 2013). The earthquakes number corresponds to 241 and 70, respectively. We then distinguish these two phases differently in the following statistical analysis.

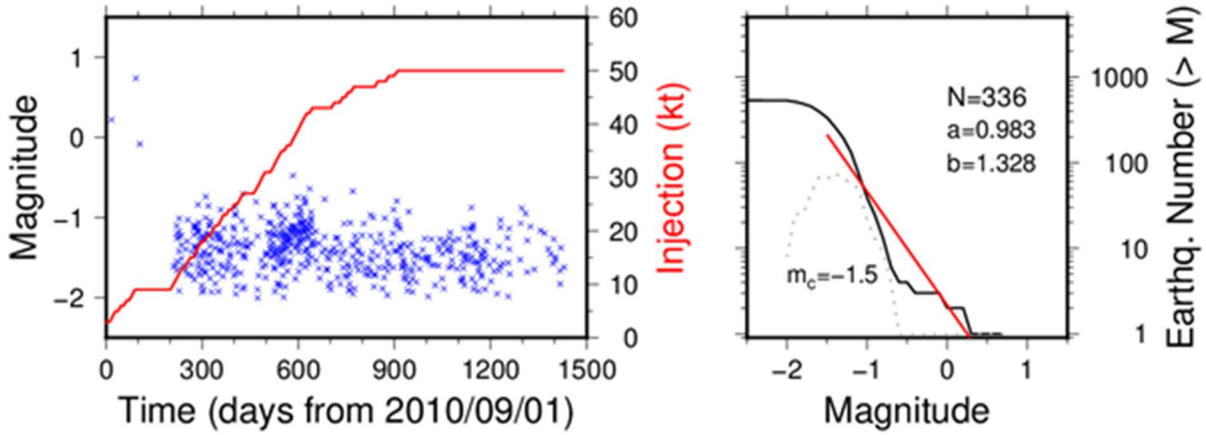

Figure 9: (left) The seismicity catalogue from Payre et al. (2014) for the Rousse CO_2 injection experiment. The injection volume is also shown for reference (total 51 kt). (right) The magnitude-frequency relation in cumulative number (black solid line) and in the number of each 0.1 magnitude (dotted line). The linear regression (red line) informs the completeness of the catalogue down to magnitude -1.5 and a b-value (slope) of about 1.3.

4.1.2 Estimation of parameters

The post-injection phase has no instantaneous influence of injection but is related only to the past process and seismicity. We apply the non-stationary seven-parameter model (chapter 3.1.1). Regardless of the small

number of earthquakes (70 events only), the regression provides a converged solution set (Figure 10). The obtained parameters are in the below table below with M_c = -1.5.

Table 1: Estimated parameters of the ETAS model

Parameter	Obtained value
μ_0	0.004 (event/day)
B	0.26 (event/day)
γ	0.048 (day^{-1})
K	0.027 (event/day)
α	1.29
c	2e-11 (day)
p	0.9

The basic parameters of the ETAS model $(\mathrm{K}, \alpha, c, p)$ are quite reasonable. This table shows that the seismicity rate is B = 0.25 (event/day) at the moment of injection end (the beginning of post-injection period), and reduces after that to 0.004 (event/day). The decay parameter B indicates that the seismicity rate is reduced by a factor 3 20 days later and divided by 20 60 days later. It is very important that the ETAS regression reveals the seismic rate change, in particular, the return to the normal seismicity rate μ_0.

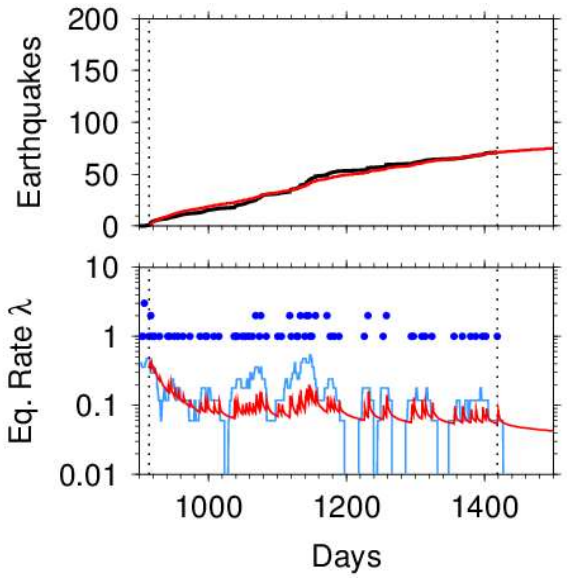

Figure 10: ***Regression result for the post injection period. (Top) The comparison of cumulative earthquake number (observation in black, ETAS model in red). (bottom) The comparison of daily earthquake numbers (blue points), averaged earthquake rate (light blue line) and earthquake rate estimated by the ETAS model (red line).***

On the other hand, it is difficult to provide a stable regression for the injection period, mainly because the seismicity rate varies with time according to the injection process and its relation is unknown. However, supposing that the basic ETAS parameters $(\mathrm{K}, \alpha, c, p)$ are unchanged during the whole period of the observation, we can estimate the parameter μ as variable, namely,

$$\mu(t) = \lambda(t) - \sum_i \mathrm{K} e^{\alpha(M_i - M_c)} \frac{1}{(t + c - t_i)^p}$$

where $\mathrm{M} = \int \lambda(t) dt$ provides the observed cumulative earthquake number and the second term on the right-hand side corresponds to the contribution of triggering (aftershock) effect of past earthquakes. Figure 11 shows

the extracted evolution of $\mu(t)$. This is a straight-forward calculation fixing the parameters $(\mathrm{K}, \alpha, c, p)$ in the standard five-parameter ETAS model.

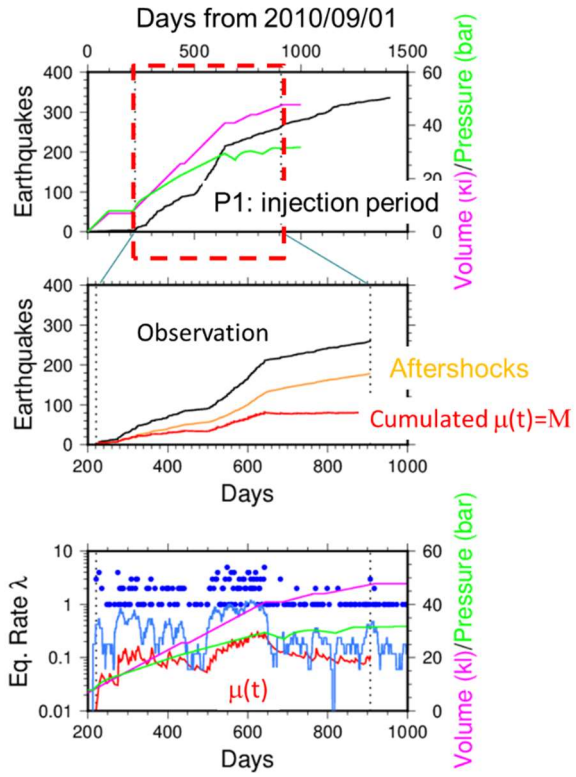

Figure 11: (top) Seismicity (black line) with the injected volume (pink) and reported pressure (green). The injected period (red broken area) is analysed. (middle) The observed cumulative earthquake numbers (black line), the calculated triggering contribution (orange) and the cumulated base rate (M as defined above). (bottom) Seismicity (blue dots), averaged seismicity rate (light blue line) and the extracted base rate (red line). The injected volume and pressure are plotted again for reference.

Finally, Figure 12 shows some attempts to correlate the detected variation of $\mu(t)$ or its integral $\mathrm{M}(t)$. It is confirmed that even during the steady injection (constant injection rate) $\mu(t)$ changes. The behaviour is similar for total injection and pressure in the current example. Both indices are visibly correlated in Figure 11, so that we should be careful when generalising. Nevertheless, it seems common that some actions activate $\mu(t)$ rapidly and then this decreases with time gradually. More analyses will be planned in the coming months.

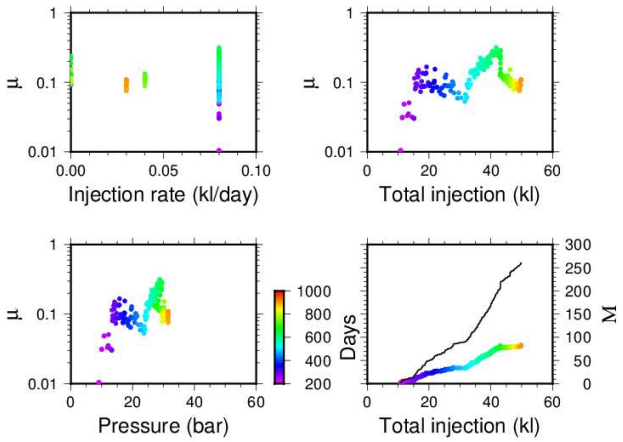

Figure 12: From top left to right bottom, variation of $\mu(t)$ with injection rate, total injection and pressure and $\mathrm{M}(t)$ with total injection. The colour represents the days shown in Figure 11.

4.1.3 Perspective

The case of Rousse is a real-world example of localised micro-seismicity due to fluid injection by a single well into a reservoir. It is still difficult to derive any explicit relation between the injection operation (injected volume and well pressure) and "ETAS de-clustered" seismicity rate during the injection. However, our attempt quantitatively indicates that the seismicity rate is decreasing by a factor of 20 after 60 days for the post-injection phase. Therefore the level of natural seismicity existing before injection is reached rapidly after the arrest of the injection.

On the other hand, the analysis also shows qualitatively that the seismicity rate is depending on the on-going operational parameters (injected volume and well pressure) during a continuous operation. However a change of operation (halt of injection, change of injection flow) may induce a different state of seismicity rate than the previous one.

These information are useful (not unique yet) for providing possible scenarios of the model parameters in forward modelling presented in section 3.1.

4.2 CASE STUDY 2 – OKLAHOMA, USA

4.2.1 The data

The activation of seismicity in Oklahoma and in the south of Kansas is a state scale phenomenon (Ellsworth, 2013). The multiple, massive injection of waste water in a deep aquifer (Arbuckle group) may have triggered basement faults at depth (e.g. Schoenball and Ellsworth, 2017). The seismicity catalogue is obtained and available through the Oklahoma Geological Survey[3]. We confirm that the completeness[4] is down to magnitude 2.3, which is a greater degree of resolution than the national catalogue of USGS. The relocation catalogue is provided by Schoenball and Ellsworth (2017), for example, but the event triggering is based on the Oklahoma Geological Survey (OGS) catalogue. We do not need the precise spatial locations, so we use the OGS catalogue from 2000/01 to 2018/11 (30386 earthquakes in total). The OGS also provides a fault database. The injection/extraction is reported monthly for each well via Oklahoma Corporation Commission, Oil and Gas Division[5]. All the publicly available data are compiled in Figure 13.

[3] http://www.ou.edu/ogs/research/earthquakes/seismicstations
[4] Completeness: the minimum magnitude above which it is thought that all earthquakes are reliably recorded. From: http://www.corssa.org/glossary (Accessed on 28/05/2020)
[5] https://www.occeweb.com/og/oghome.htm

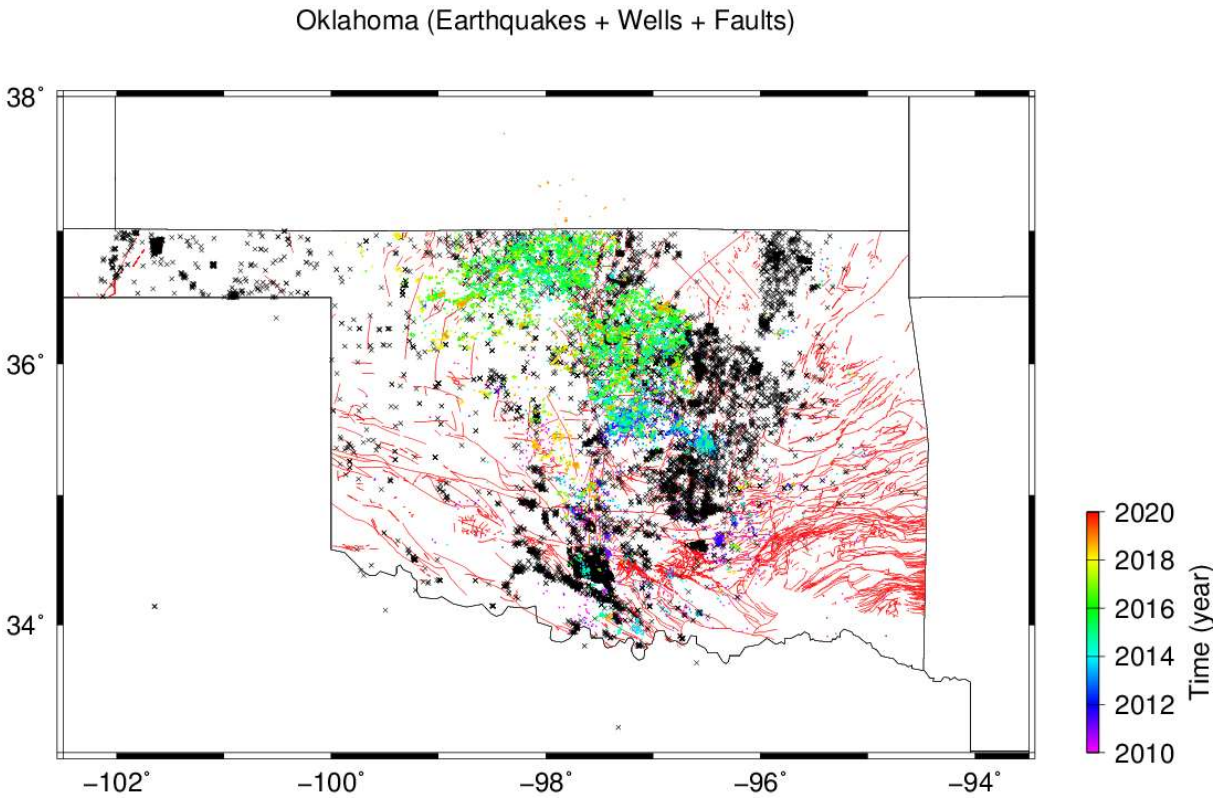

Figure 13: ***The compiled earthquakes, well positions and faults in Oklahoma state. Earthquakes are coloured by time. The injection points as of 2018 are shown by black crosses. The faults are illustrated by red lines.***

4.2.2 Estimation of parameters

First of all, we study four major earthquakes in Oklahoma:

- 2011/11/06 M5.8 Prague
- 2016/02/13 M5.1 Fairview
- 2016/09/03 M5.8 Pawnee
- 2016/11/07 M5.0 Cushing

Each of the earthquakes is accompanied by aftershocks. The area and the number of earthquakes are quite different from each other, but the regression for the five-parameter ETAS model provides a stable convergence on the parameters (α, c, p) and indicates possible variation of the parameter μ. Figure 14 shows an example for the 2011 Prague earthquake. We then fix the three parameters $(\alpha = 1.78, c = 0.011, p = 1)$ and let (K, μ) variable.

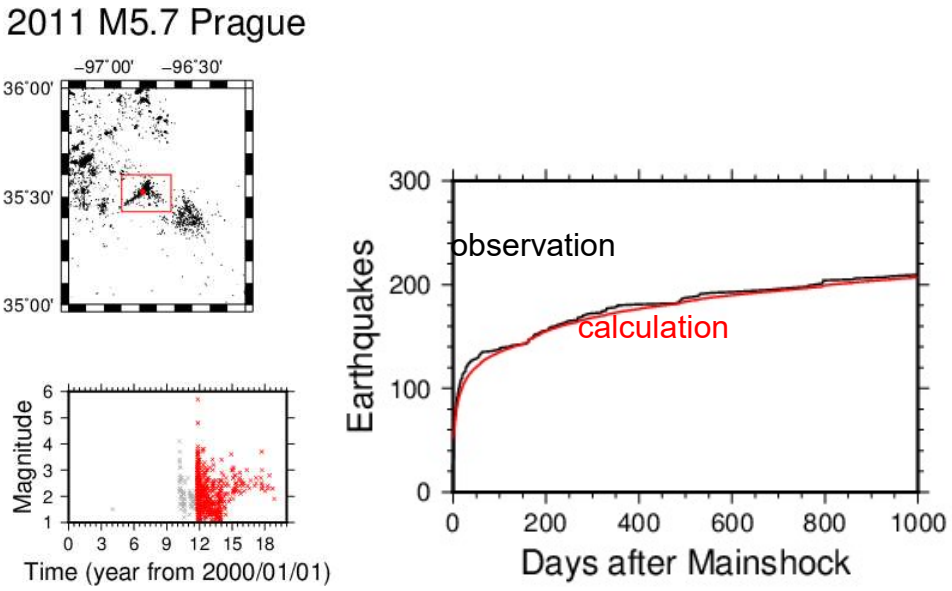

Figure 14: ***(left) 2011 Prague earthquake and regional seismicity. Red frame indicates the selected area for the analysis. Only the period after the mainshock is analysed. (right) Comparison of earthquake number between the observation and the estimation from ETAS model*** $(\alpha = 1.88, c = 0.026, p = 1, K = 0.014, \mu = 0.0070)$.

Instead of focusing on the particular area of the major earthquake, we aim to carry out systematic parameter studies. As we need a sufficient number of earthquakes for the statistics, we choose a radius of 20 km such that we have 53 areas containing at least 250 earthquakes of magnitude $M_c \geq 2.3$ (Figure 15). For all the areas, we apply the regression from the ETAS model by fixing the three parameters (α, c, p). Figure 16 shows all the results. The analyses are held for 200 events by shifting 50 events each time. Globally we find that the parameter K is unchanged in space and time. On the other hand, the parameter μ changes with time, not always proportional to the observed seismicity rate λ. In general, the seismicity shows an increase in recorded events around the year 2015, thus both λ and μ have a peak there and decrease toward 2018.

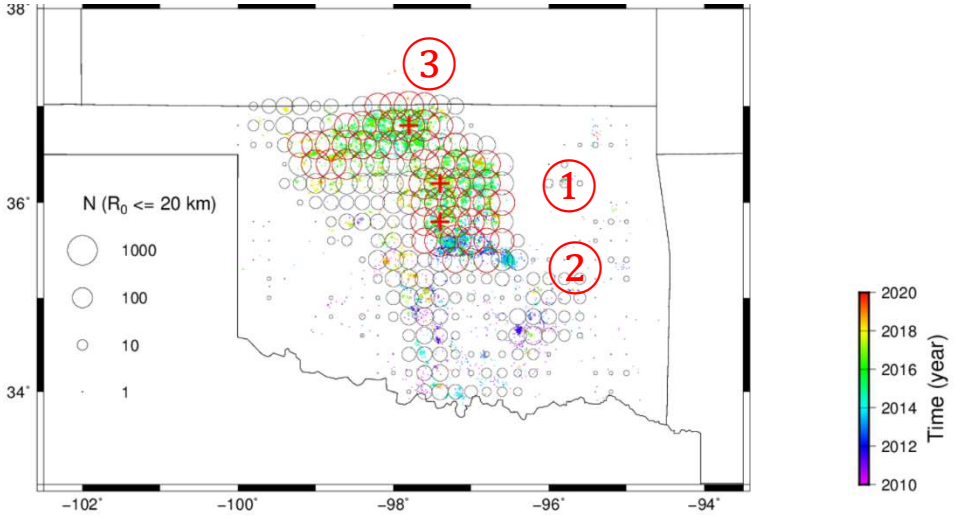

Figure 15: Evaluation of earthquake numbers every 0.2° within a radius of R0 = 20 km. The red circles show areas which include equal to or more than 250 earthquakes of magnitude Mc ≥2.3. Three marked places show the three areas with the highest seismicity.

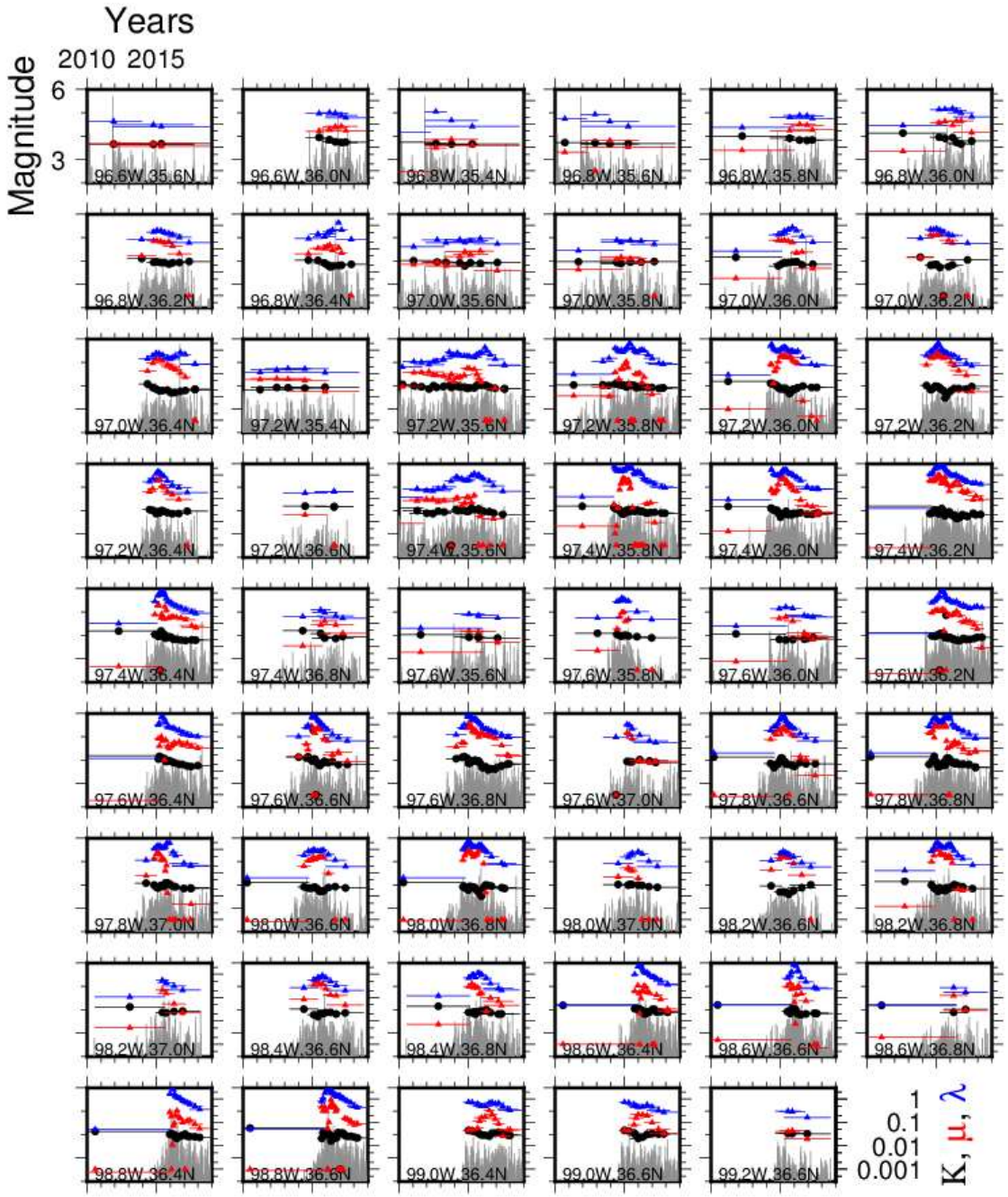

Figure 16: ETAS model fitting for 53 areas. 200 events are used every time by shifting 50 events. The seismicity is in black (magnitude and time). The observed seismicity rate $\lambda(t)$ is in blue. The obtained two parameters $(\mathrm{K}(\mathrm{t}), \mu(t))$ are in black and red, respectively. The horizontal bars correspond to the period of 200 events used for each analysis and the points represent the middle of this period.

Finally, we also extract similarly the injection information in the same area and compare with the ETAS parameters. Figure 17 represents an area, for example. As already pointed out for Figure 16, the parameter K is stable over the whole period, but the parameter μ changes with time. Especially μ becomes high at the beginning of the onset of the seismicity and decreases with time. This trend is not the same as the observed seismicity rate λ. The visible peak of λ at the end of 2015 is delayed comparing to the peak of μ. For the purpose of relating the injection parameter and the seismicity, Figure 18 plots the peak values from each area, (λ, μ) and maximum monthly injection, maximum well pressure and total injection at the moment of the peak of μ. The correlation with the maximum observed seismicity rate λ and injection is not clear (black line), while the parameter μ has a clearer, positive correlation with the injection (maximum monthly injection and total volume). The relation with the maximum well pressure in the area has positive correlation. Note that there are

still three areas where there are no wells but seismicity is triggered. This infers that the seismicity is triggered not only from the locally injected fluid but remotely due to the fluid and/or seismicity migration from the neighbours. The regression of the parameters should be related both the local operation (injected volume) and the surrounding seismicity (Aochi et al., in preparation, 2020).

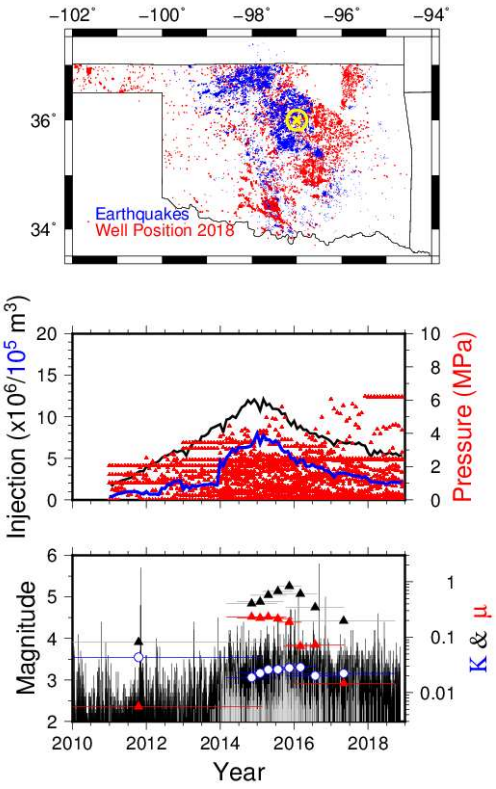

Figure 17: (top) Seismicity (blue) and well position (red). Selected area indicated by yellow mark. (middle) Injection information. Black line shows the monthly injected volume over the whole Oklahoma state. Blue line indicates the quantity in the selected area. Well pressures are marked by red for all the wells included in the selected area. (bottom) The whole seismicity in Oklahoma in black vertical bars. White bars correspond the one in the selected area used for the ETAS parameter estimation. The black, red, and blue marks with horizontal bars represent the estimation of the parameters in this selected area (same as Figure 16).

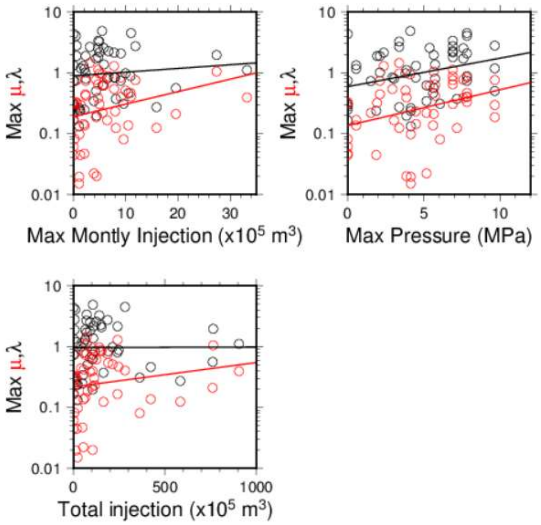

Figure 18: **Maximum values of (λ, μ) from 53 areas as a function of maximum monthly injection, maximum well pressure and total injection before the peak of μ. The linear regressions are superposed.**

4.2.3 Perspectives

The induced seismicity in Oklahoma is another extreme end case where many faults are activated regionally due to massive fluid injection from many wells (Ellsworth, 2015). The ETAS declustering analysis clearly shows drastic increase of seismicity rate from 2013 to 2015. Our analysis confirms a decrease of seismicity after the peak (2015-2016) toward the end of 2018. Although further quantitative analysis is a continuous task, we have learnt:

- The seismicity change is due not only to the local injections but also the migration of fluid or/and seismicity from the surrounding, since there are very few injections in some areas regardless of the activation of seismicity.
- Triggering rate (K) is quasi-steady during the whole period and over the whole area. A slight gradual decrease by a factor of 2 at average is important for anticipating the long-term seismicity evolution once activated.

We also note

- ETAS declustered seismicity rate is not always proportional to the observed seismicity rate ($\mu/\lambda \neq constant$). Therefore it is important to detect the change of μ to forecast the seismicity.

A systematic study between the injection parameters and the seismicity in different contexts remains a future work. The two demonstrative examples in this chapter will give basis to accumulate the experience and estimate the model parameters for assessing the seismicity evolution.

4.3 DATA AND RESOURCES

In this project, we have used publicly accessible data sets from different published examples. The Rousse data can be obtained in the paper of Payre et al. (2014). The Oklahoma data are available from Oklahoma Geological Survey for the seismicity catalogue (http://www.ou.edu/ogs/research/earthquakes/seismicstations) and from Oklahoma Corporation Commission, Oil and Gas Division for the injections (https://www.occeweb.com/og/oghome.htm). The codes of ETAS analysis are available from Institute of Statistical Mathematics, Japan (https://www.ism.ac.jp/index.html).

5 Discussion and perspectives

Firstly, what is evident from the previous chapters is that the interaction of mechanisms leading to induced seismicity is complex and thus to accurately model the interacting processes is very challenging. Based on the literature review it is clear that models respond to several objectives and that it is challenging, if not impossible, to find a "one size fits all" tool, which explains the great variety of approaches. Broadly, here is a list of objectives for modelling activities:

- Provide prediction capacities in order to guide decision making and/or risk management. This can be further divided into:
    - Short-term forecasting, with a scale in the order of an hour. This requires very fast models that are constantly recalibrated using real-time data.
    - Long-term forecasting, with a scale on the order of months. This requires more robust models which can reproduce a larger variety of scenarios. They however do not need to be as fast as for short-term forecasting
- Provide insights into the underlying mechanisms of induced seismicity: these models are necessarily physics-based and may be large and complex.

Following the subdivision of models introduced in chapter 2, it is evident that statistical models are primarily useful for short-term forecasting, and that complex physics-based models are primarily more suited for providing insights. It is less clear which type of models is most useful for long-term forecasts and this is where hybrid models have emerged and seem to be a promising option.

Consequently, we can only assess which model is the "best" for a given application, and assessment of the optimum model depends on the objectives of the modelling approach.

Regarding forecasting applications, methods have been developed for rigorously benchmarking models. Such methods have been proposed for instance by Király-Proag et al. (2016). In this paper they compute a log-likelihood of obtaining the data based on the models. There are other indicators which can be more suited to a probabilistic approach such as the Brier score used for instance in weather forecasting (Brier, 1950). However, the precision in prediction should be balanced with the complexity of the model to maintain realistic computation times and to reduce the risk of overfitting[6]. This is typically achieved by using widely used criteria for model selection such as the Akaike information criterion or the Bayes factor (Claeskens, 2016). The approach of rigorous model selection should not be restricted to statistical models but also to physics-based models (at least when used for forecasting).

The literature review revealed that very few papers formally compare the performance of different models. Even when several models are tested, the authors do not generally conclude on a best model. In this regard, the approach followed by Mena et al. (2013) is interesting because instead of choosing a "best" model, they build an ensemble model by combining several models using weights computed with one of the aforementioned model selection criteria.

From the review, it is also clear that currently no model is able to predict future seismicity without a calibration phase first, in order to determine uncertain parameters. This means that the quality and the availability of the data collected is very important in order to ensure the best quality from the models.

In this respect, the most challenging aspect is for short-term forecasting where data is needed to be collected and interpreted in real-time. Another important aspect is that parameter inference relies primarily on maximizing the log likelihood, which is a method that works best with a lot of data. This is a problem particularly in the context of CO_2 storage where levels of induced seismicity are expected to be relatively low. A solution is to use a Bayesian framework for parameters inference (e.g. Broccardo et al. 2017; Wang et al. 2016). In this framework, the modeller needs to explicitly model the prior information, which is then updated using Bayes formula with each data point. This provides better results in small data situations (as opposed to big data) and provides results as distributions, which allows more flexibility for decision making. The main drawback is the added complexity during inference as it relies on sampling methods such as the Monte Carlo Markov Chain method.

[6] In statistics, **overfitting** is "the production of an analysis that corresponds too closely or exactly to a particular set of data, and may therefore fail to fit additional data or predict future observations reliably" - https://en.wikipedia.org/wiki/Overfitting

Regarding possible future work, there are plenty of possible directions. In the scope of SECURe, the work on physics-based modelling will be extended in deliverables D2.5 and D2.6, and the decision workflow will be further developed in WP5.

The application of the ETAS model to the Rousse dataset could be further improved by testing a Bayesian inference (as there are relatively few events) of the parameters and potentially comparing different models (e.g. ETAS vs seismogenic index) using model selection criteria as mentioned above.

The Oklahoma case is quite complex and challenging, and there are many possibilities that we can explore: using a spatio-temporal version of the ETAS model, using a hybrid version of the ETAS model, using a calibrated ETAS model to test predictions for future injection scenarios. This last idea can be quite challenging because the ETAS model can be quite unstable, meaning that if it predicts a large event, its aftershock sequence will dominate the seismicity rate. This means that in a Monte Carlo simulation, the results can be very different from one simulation to the next so predictions come with a lot more uncertainty than with other types of models.

Finally, an additional deliverable for this project would be to improve our current toolbox by incorporating different models, giving the possibility to infer parameters from data, and to run forward models for forecasts.

These ideas were not initially planned within the SECURe project and are propositions for future work.

6 Conclusions

- The science of induced seismicity is very complex and relies on many interacting processes
- Modelling approaches have been grouped in three categories:
    - Statistical approaches seek to fit a mathematical model to a set of data and will be more used in short-term forecasting
    - Physics-based approached seek to reproduce the underlying interacting phenomena and mainly are used for increasing understanding
    - Hybrid-approaches use a combination of the previous approaches and are promising for longer-term forecasts
- The ETAS model (for Epidemic Type Aftershock Sequence) is a widely used statistical model for fitting and declustering natural catalogues, and was adapted to induced seismicity in the context of deep geothermal energy
- We apply this model to two case studies, a small-scale pilot of CO_2 injection and a large-scale regional wastewater injection case.
- Both case studies show a clear relationship between operations and observed seismicity
- However the relationships show non-linear effect and it remains a challenge to find an adequate mathematical representation of this relationship

7 References

Aochi et al. (2017) Developing subsurface energy exploitation strategies by considering seismic risk, Petrol. Geosci., 23, 298-305, https://doi.org/10.1144/petgeo2016-065 .

Bachmann, C. E., Wiemer, S., Woessner, J., & Hainzl, S. (2011). Statistical analysis of the induced Basel 2006 earthquake sequence: introducing a probability-based monitoring approach for Enhanced Geothermal Systems. Geophysical Journal International, 186(2), 793-807.

Baisch, S., Voros, R., Rother, E., Stang, H., Jung, R., Schellschmidt, R., 2010. A numerical model for fluid injection induced seismicity at Soultz-sous-Forêts. Int. J., Rock Mech. Min. Sc. 47 (3), 405-413.

Bommer, J. J., Oates, S., Cepeda, J. M., Lindholm, C., Bird, J., Torres, R., ... & Rivas, J. (2006). Control of hazard due to seismicity induced by a hot fractured rock geothermal project. Engineering Geology, 83(4), 287-306.

Bommer, J. J., Crowley, H., & Pinho, R. (2015). A risk-mitigation approach to the management of induced seismicity. Journal of Seismology, 19(2), 623-646.

Bourne, S. J., & Oates, S. J. (2017). Development of statistical geomechanical models for forecasting seismicity induced by gas production from the Groningen field. Netherlands Journal of Geosciences, 96(5), s175-s182.

Brier, G. W. (1950). Verification of forecasts expressed in terms of probability. Monthly weather review, 78(1), 1-3.

Broccardo, M., Mignan, A., Wiemer, S., Stojadinovic, B., & Giardini, D. (2017). Hierarchical Bayesian modeling of fluid-induced seismicity. Geophysical Research Letters, 44(22), 11-357.

Buijze, L., Orlic, B., Wassing, B. B. T., & Schreppers, G.-J. (2015, November 13). Dynamic Rupture Modeling of Injection-Induced Seismicity: Influence of Pressure Diffusion Below Porous Aquifers. American Rock Mechanics Association.

Buijze, L., van Bijsterveldt, L., Cremer, H., Paap, B., Veldkamp, H., Wassing, B., ter Heege, J., 2019a. review of worldwide geothermal projects: mechanisms and occurrence of induced seismicity. TNO-report 2019 R100043. http://www.nlog.nl/sites/default/files/2019-09/worldwidegeothermalprojectsrelationinducedseismicity-tno-2019-r10043.pdf

Buijze, L., van den Bogert, P.A.J., Wassing, B.B.T., Orlic, B., 2019b. Nucleation and Arrest of Dynamic Rupture Induced by Reservoir Depletion. Journal of Geophysical Research: Solid Earth, 124, 3620-3645. https://doi.org/10.1029/2018JB016941.

Candela,T., Ampuero, J.P., Van Wees, J-D, Fokker, P., Wassing, B., 2019a. Semi-analytical fault injection model: effect of fault roughness and injection scheme on induced seismicity. European Geothermal Congress 2019, Den Haag, The Netherlands, 11-14 June 2019.

Candela, T., Osinga, S., Ampuero, J.-P., Wassing, B., Pluymaekers, M., Fokker, P.A., et al. (2019b). Depletion-induced seismicity at the Groningen gasfield: Coulomb rate-and-state models including differential compaction effect. Journal of Geophysical research: Solid earth, 124, 7081-7104.

Claeskens, G. (2016). Statistical model choice. *Annual review of statistics and its application*, *3*, 233-256.

Clarke, H., Verdon, J. P., Kettlety, T., Baird, A. F., & Kendall, J. M. (2019). Real-Time Imaging, Forecasting, and Management of Human-Induced Seismicity at Preston New Road, Lancashire, England. Seismological Research Letters, 90(5), 1902-1915.\

Davies, R., Foulger, G., Bindley, A., Styles, P. (2013). Induced seismicity and hydraulic fracturing for the recovery of hydrocarbons: Marine and Petroleum Geology, 45, 171-185.

Dempsey, D., & Riffault, J. (2019). Response of induced seismicity to injection rate reduction: Models of delay, decay, quiescence, recovery, and Oklahoma. Water Resources Research, 55(1), 656-681.

Dieterich, J.: A constitutive law for rate of earthquake production and its application to earthquake clustering. J. of Geophys. Research (1994), 99 B2, 2601-2618.

Ellsworth, W.L. (2013) Injection-induced earthquakes, Science, 341, 6142, doi:10.1126/science.1225942.

Fokker, P.A., Wassing, B.B.T., 2019. A fast model for THM processes in geothermal applications. European Geothermal Congress 2019, Den Haag, The Netherlands, 11-14 June 2019.

Energy Post. « UK Fracking Earthquakes: Why the World's "Toughest" Safety Rules Failed to Predict Them », 11 septembre 2019. https://energypost.eu/uk-fracking-earthquakes-why-the-worlds-toughest-safety-rules-failed-to-predict-them/.

Gaucher, E., Schoenball, M., Heidbach, O., Zang, A., Fokker, P. A., van Wees, J. D., & Kohl, T. (2015). Induced seismicity in geothermal reservoirs: A review of forecasting approaches. Renewable and Sustainable Energy Reviews, 52, 1473-1490.

Gischig, V. S., & Wiemer, S. (2013). A stochastic model for induced seismicity based on non-linear pressure diffusion and irreversible permeability enhancement. Geophysical Journal International, 194(2), 1229-1249.

Goertz-Allmann, B. P., & Wiemer, S. (2013). Geomechanical modeling of induced seismicity source parameters and implications for seismic hazard assessment. Geophysics, 78(1), KS25-KS39

Hainzl & Ogata (2005) Detecting fluid signals in seismicity data through statistical earthquake modeling, JGR, 110, B05S07, https://doi.org/10.1029/2004JB003247.

Hallo, M., Oprsal, I., Eisner, L., & Ali, M. Y. (2014). Prediction of magnitude of the largest potentially induced seismic event. Journal of seismology, 18(3), 421-431.

Häring, M. O., Schanz, U., Ladner, F., & Dyer, B. C. (2008). Characterisation of the Basel 1 enhanced geothermal system. Geothermics, 37(5), 469-495.

Heimisson, E. R., & Segall, P. (2018). Constitutive law for earthquake production based on rate-and-state friction: Dieterich 1994 revisited. *Journal of Geophysical Research: Solid Earth*, 123, 4141– 4156. https://doi.org/10.1029/2018JB015656

Jin and Zoback, 2018. Fully Dynamic Spontaneous Rupture Due to Quasi-Static Pore Pressure and Poroelastic effects: An Implicit Nonlinear Computational Model of Fluid-Induced Seismic Events. Journal of Geophys. Res. – Solid Earth, Vol. 123, Issue 11, 9430-9468.

Király-Proag, E., Zechar, J. D., Gischig, V., Wiemer, S., Karvounis, D., & Doetsch, J. (2016). Validating induced seismicity forecast models—Induced seismicity test bench. Journal of Geophysical Research: Solid Earth, 121(8), 6009-6029.

Langenbruch, C., & Zoback, M. D. (2016). How will induced seismicity in Oklahoma respond to decreased saltwater injection rates?. Science advances, 2(11), e1601542.

Langenbruch, C., Weingarten, M., & Zoback, M. D. (2018). Physics-based forecasting of man-made earthquake hazards in Oklahoma and Kansas. Nature communications, 9(1), 1-10.

Llenos, A. L., & Michael, A. J. (2013). Modeling earthquake rate changes in Oklahoma and Arkansas: Possible signatures of induced seismicity. Bulletin of the Seismological Society of America, 103(5), 2850-2861.

Madiaraga, R., 1979. On the Relation Between Seismic Moment and Stress Drop in the Presence of Stress and Strength Heterogeneity. Journal of Geophysical Research, Vol.84, No.B5.

Maury, J., Aochi, H., Ben Rhouma, S., & Le Guenan, T. (2019). Detecting seismicity rate variation using ETAS model for induced seismicity, AGU fall meeting, S23E-0681, San Francisco, USA, December 2019.

McGarr (2014) Maximum magnitude earthquakes induced by fluid injection, J. Geophys. Res., 119, 1008-1019, http://doi.org/10.1002/2013JB010597.

Mena, B., Wiemer, S., & Bachmann, C. (2013). Building robust models to forecast the induced seismicity related to geothermal reservoir enhancement. Bulletin of the Seismological Society of America, 103(1), 383-393.

Mignan, A., Broccardo, M., Wiemer, S., & Giardini, D. (2017). Induced seismicity closed-form traffic light system for actuarial decision-making during deep fluid injections. Scientific reports, 7(1), 1-10.

Mitchell, J. K., & Green, R. A. (2017). Some induced seismicity considerations in geo-energy resource development. Geomechanics for Energy and the Environment, 10, 3-11.

Mortezaei, K., & Vahedifard, F. (2015). Numerical simulation of induced seismicity in carbon capture and storage projects. Geotechnical and Geological Engineering, 33(2), 411-424.

Norbeck, J. H., & Rubinstein, J. L. (2018). Hydromechanical earthquake nucleation model forecasts onset, peak, and falling rates of induced seismicity in Oklahoma and Kansas. Geophysical Research Letters, 45(7), 2963-2975.

Ogata (1983) Estimation of the parameters in the modified Omori formula for aftershock frequencies by the maximum likelihood procedure, J. Phys. Earth, 31, 115-124.

Ogata (1988) Statistical models of point occurrences and residual analysis for point processes, J. Am. Stat. Assoc., 83, 9-27.

Ogata, Y., & Zhuang, J. (2006). Space–time ETAS models and an improved extension. *Tectonophysics*, *413*(1-2), 13-23.

Okutani & Ide (2011) Statistic analysis of swarm activities around the Boso Peninsula, Japan: Slow slip events beneath Tokyo Bay?, EPS, 63, 419-426, https://doi.org/10.5047/eps.2011.02.010.

Payre, X., Maison, C. Marblé, A., Thibeau, S. (2014) Analysis of the passive seismic monitoring performance at the Rousse CO2 storage demonstration pilot, Energy Procedia, 63, 4339-4357, https://doi.org/10.1016/j.egypro.2014.11.469.

Porter, R. T., Striolo, A., Mahgerefteh, H., & Faure Walker, J. (2019). Addressing the risks of induced seismicity in subsurface energy operations. Wiley Interdisciplinary Reviews: Energy and Environment, 8(2), e324.

Rinaldi, A. P., Rutqvist, J., & Cappa, F. (2014). Geomechanical effects on CO2 leakage through fault zones during large-scale underground injection. International Journal of Greenhouse Gas Control, 20, 117-131.

Rutqvist, J., Cappa, F., Rinaldi, A. P., & Godano, M. (2014). Modeling of induced seismicity and ground vibrations associated with geologic CO2 storage, and assessing their effects on surface structures and human perception. International Journal of Greenhouse Gas Control, 24, 64-77.

Schoenball, M. & Ellsworth, W.L. (2017) A systematic assessment of the spatiotemporal fault activation through induced seismicity in Oklahoma and Southern Kansas, J. Geophys. Res., 122, 10189-10206. Doi:10.1002/2017JB014850.

Segall, P., & Lu, S. (2015). Injection-induced seismicity: Poroelastic and earthquake nucleation effects. Journal of Geophysical Research: Solid Earth, 120(7), 5082-5103.

Shapiro, S. A., Dinske, C., Langenbruch, C., & Wenzel, F. (2010). Seismogenic index and magnitude probability of earthquakes induced during reservoir fluid stimulations. The Leading Edge, 29(3), 304-309.

Stamatelatos, M., Dezfuli, H., Apostolakis, G., Everline, C., Guarro, S., Mathias, D., ... & Vesely, W. (2011). Probabilistic risk assessment procedures guide for NASA managers and practitioners.

Taron, J., Elsworth, D., & Min, K. B. (2009). Numerical simulation of thermal-hydrologic-mechanical-chemical processes in deformable, fractured porous media. *International Journal of Rock Mechanics and Mining Sciences*, *46*(5), 842-854. https://doi.org/10.1016/j.ijrmms.2009.01.008

Ter Heege, J., Osinga, S., Wassing, B., Candela, T., Orlic, B., Buijze, L., Chitu, A. (2018). Mitigating induced seismicity around depleted gas fields based on geomechanical modeling. The Leading Edge, 37(5), 322–400.

Thibeau, S, Chiquet P, Prinet C, Lescanne M. (2013) Lacq-Rousse CO2 Capture and Storage demonstration pilot: Lessons learnt from reservoir modelling studies. Energy Procedia; 37, 6306-6316.

van Stiphout, T., Zhuang, J., & Marsan, D. (2012). Seismicity declustering. *Community Online Resource for Statistical Seismicity Analysis*, *10*(1).

Van Wees, J-D., Pluymaekers, M., Osinga, S., Fokker, P., Van Thienen-Visser, K., Orlic, B., Wassing, B., Hegen, D., Candela, T, 2019. 3-D mechanical analysis of complex reservoir: a novel mesh-free approach. Geophys. J. Int. (2019b), 1118-1130.

Verdon, J. P., Kendall, J. M., White, D. J., & Angus, D. A. (2011). Linking microseismic event observations with geomechanical models to minimise the risks of storing CO2 in geological formations. Earth and Planetary Science Letters, 305(1-2), 143-152.

Verdon, J. P., Stork, A. L., Bissell, R. C., Bond, C. E., & Werner, M. J. (2015). Simulation of seismic events induced by CO2 injection at In Salah, Algeria. Earth and Planetary Science Letters, 426, 118-129.

Verdon, J. P., & Budge, J. (2018). Examining the capability of statistical models to mitigate induced seismicity during hydraulic fracturing of shale gas reservoirs. Bulletin of the Seismological Society of America, 108(2), 690-701.

Vilarrasa, V., Carrera, J., Olivella, S., Rutqvist, J., & Laloui, L. (2019). Induced seismicity in geologic carbon storage. Solid Earth (online), 10(3).

Walsch F.R. and Zoback, M.D., 2016. Probabilistic assessment of potential fault slip related to injection-induced earthquakes: Application to north-central Oklahoma, USA, Geology (2016) 44 (12): 991-994.

Wang, P., Small, M. J., Harbert, W., & Pozzi, M. (2016). A Bayesian approach for assessing seismic transitions associated with wastewater injections. Bulletin of the Seismological Society of America, 106(3), 832-845.

Wang, P., Small, M. J., Harbert, W., & Pozzi, M. (2017). Spatially distributed non-stationary seismic hazard. Safety, Reliability, Risk, Resilience and Sustainability of Structures and Infrastructure. 12th Int. Conf. on Structural Safety and Reliability, Vienna, Austria, 6–10 August 2017

Wassing, B. B. T., Buijze, L., & Orlic, B. (2016, June). Modelling of fault reactivation and fault slip in producing gas fields using a slip-weakening friction law. In *50th US Rock Mechanics/Geomechanics Symposium*. American Rock Mechanics Association.

White, J. A., & Foxall, W. (2016). Assessing induced seismicity risk at CO2 storage projects: Recent progress and remaining challenges. International Journal of Greenhouse Gas Control, 49, 413-424.

Zhai, G., Shirzaei, M., Manga, M., & Chen, X. (2019). Pore-pressure diffusion, enhanced by poroelastic stresses, controls induced seismicity in Oklahoma. Proceedings of the National Academy of Sciences, 116(33), 16228-16233.

Zhuang, J., Harte, D., Werner, M. J., Hainzl, S., & Zhou, S. (2012). Basic models of seismicity: Temporal models. Community Online Resource for Statistical Seismicity Analysis, 33.